Quantitative MRI as a Biomarker of Disease Severity in Neuromuscular Disease

Tanay Satarkar

Thesis submitted to the University of Ottawa
in partial Fulfillment of the requirements for the
Master of Science in Neuroscience

Department of Cellular and Molecular Medicine
Faculty of Medicine
University of Ottawa

Thesis abstract

Introduction: Oculopharyngeal muscular dystrophy (OPMD) is a slowly progressive disorder marked by ptosis, dysphagia, and proximal muscle weakness. Reliable biomarkers for monitoring are limited, making progression difficult to track in clinics and future trials. Quantitative MRI (qMRI), particularly fat-fraction (FF) and water measures offer a non-invasive way to assess muscle involvement and follow change over time.

Aim: To evaluate 97 muscles in OPMD using qMRI and determine if diffusion-related MRI markers [apparent diffusion coefficient (ADC) intravoxel incoherent motion (IVIM)], and T2 relaxation time identify earlier signs of disease activity compared to muscle FF.

Methods: The study included 52 participants, 40 patients with OPMD and 12 controls with whole body 3T qMRI. For FF and ADC, 97 muscles were segmented and 24 thigh muscles were segmented for IVIM and T2 map using ITK SNAP version 3.8.0. Statistical analyses used GraphPad Prism and R-studio using, Wilcoxon unpaired tests and Spearman correlation $p < 0.05$.

Results: Muscles such as adductor magnus (41.2±28.9 %), soleus (39.2±25.9 %), and biceps femoris long head (BL) (33.8±25.2 %), showed higher FF. Higher FF was linked to a stronger negative correlation between FF-ADC, adductor magnus (spearman's $\rho = -0.90$), soleus (spearman's $\rho = -0.83$), biceps femoris long head (spearman's $\rho = -0.87$)), and FF-IVIM true diffusion (spearman's $\rho = -0.89$ CI, -0.94, -0.80 respectively). IVIM perfusion-fraction correlated positively with FF in adductor magnus and biceps femoris long head (spearman's $\rho = 0.80$) in the early disease duration period (0-5 years). Exploratory disease-duration stratification showed ADC did not rise prior to fat replacement, as might occur with inflammation and edema; instead, ADC decreased as fat replacement increased.

Discussion: FF is a sensitive marker of disease severity and shows a strong negative correlation with diffusivity markers. In this cross-sectional analysis, diffusion values do not rise before fat replacement onset. Identifying sensitive biomarkers of OPMD severity and disease progression is important to identify treatment windows for future trials.

Acknowledgement

I would like to express my sincere gratitude to my supervisors, Dr. Jodi Warman-Chardon and Dr. Gerd Melkus, for their guidance, support, and mentorship throughout this thesis. Their expertise in neuromuscular disease, quantitative MRI, and clinical research has been essential in shaping this project. It has been a true privilege to have the opportunity to work on a cutting-edge project under the supervision of mentors whose work I have long admired and with whom I had hoped to work for many years. I am deeply grateful for the time, feedback, and encouragement they have provided during each stage of this work.

I would also like to thank my thesis advisory committee members for their valuable input and thoughtful suggestions, which have been the backbone on which this thesis was developed.

I am grateful to the Ottawa Neuromuscular Imaging group and the Neuromuscular Centre at The Ottawa Hospital for providing a supportive research environment. I would like to thank the clinical and research team members who contributed to participant recruitment, imaging, data organization, and image analysis. I am especially thankful to Dr. Marcos Sampaio for his support with review of the muscle segmentation levels and radiological guidance. I would also like to thank Dr. Ian Smith for his invaluable guidance and direction with the data analysis, poster making sessions.

I would also like to acknowledge all participants with OPMD and the control participants who contributed to this study. Their participation made this research possible and will hopefully contribute to improved understanding of OPMD and future clinical trial studies.

TABLE OF CONTENTS

Table of Contents

List of abbreviations

ADC	Apparent diffusion coefficient
BH-FDR	Benjamini–Hochberg false discovery rate
CK	Creatine kinase
D	Diffusion coefficient
D*	Pseudo-diffusion coefficient
DICOM	Digital Imaging and Communications in Medicine
DWI	Diffusion-weighted imaging
FF	Fat fraction
f	Perfusion fraction
GCN	Guanine-cytosine-trinucleotide repeat
IVIM	Intravoxel incoherent motion
ITK-SNAP	Insight Toolkit-SNAP
LOESS	Locally estimated scatterplot smoothing
MRC	Medical Research Council
MRI	Magnetic resonance imaging
NMD	Neuromuscular disease
OPMD	Oculopharyngeal muscular dystrophy
PABPN1	Polyadenylate-binding protein nuclear 1
PACS	Picture Archiving and Communication System
qMRI	Quantitative magnetic resonance imaging
ROI	Region of interest
SNR	Signal-to-noise ratio
STIR	Short T1 inversion recovery
T	Tesla
T2	Transverse relaxation time
TE	Echo time
TSE	Turbo spin echo
VIBE	Volumetric interpolated breath-hold examination

List of Figures

right sides averaged for each muscle. Comparisons were performed using unpaired Wilcoxon tests for each muscle, with Benjamini–Hochberg false discovery rate (BH-FDR) correction applied across thigh muscles. P values displayed above each muscle correspond to BH-FDR-adjusted values; ** indicates BH-FDR $p < 0.05$.

Figure 5: Relationship between FF and ADC across thigh muscles in OPMD participants: Stronger negative correlation in high FF muscles: Figure 3A exhibits the association between FF and ADC across thigh muscles in patients with OPMD. Each point represents a muscle-level measurement. Overall, FF and ADC showed a moderate negative correlation (Spearman $\rho = -0.55$), indicating lower ADC values with increasing fat replacement. The table in Figure 3B represents: Individual muscle summary of mean FF, Spearman correlation coefficients, and Bonferroni-corrected p values for the association between FF and ADC in individual thigh muscles. Figure 3A indicates as the FF increases the diffusivity decreases, and the negative correlation strength is stronger in higher FF muscles as shown in the Table 3B.

Figure 6: Apparent diffusion coefficient differences in high FF thigh muscles between OPMD participants and controls. Each point represents an individual muscle measurement, with left and right sides averaged for each muscle. Comparisons were performed using unpaired Wilcoxon tests for each muscle, with Benjamini–Hochberg false discovery rate (BH-FDR) correction applied across thigh muscles. P values displayed above each muscle correspond to BH-FDR-adjusted values; ** indicates BH-FDR $p < 0.05$. Muscles such as the adductor magnus and biceps femoris showed lower ADC values in OPMD than in controls, while several other thigh muscles showed a nonsignificant difference.

Figure 7: Correlation between FF and IVIM D: Figure 5A scatter plot showing the relationship between FF and IVIM D across thigh muscles in patients with OPMD. Each point represents a muscle-level measurement. Overall, FF and IVIM D showed a moderate negative correlation (Spearman $\rho = -0.63$), indicating lower diffusivity with increasing fat replacement. The table in Figure 5B represents: Individual muscle mean FF, Spearman correlation coefficients, and Bonferroni-corrected p values for the association between FF and IVIM D in individual thigh muscles showing a strong negative correlation between FF-IVIM D in highly fat replaced muscles.

Figure 8: IVIM (D) differences between OPMD group and controls when assessing high FF muscles of thigh region. Each point represents an individual muscle measurement, with left and right sides averaged for each

muscle. Comparisons were performed using unpaired Wilcoxon tests for each muscle, with (BH-FDR) correction applied across thigh muscles. P values displayed above each muscle correspond to BH-FDR-adjusted values; ** indicates BH-FDR $p < 0.05$. The figure shows that muscles with greater fat replacement, including adductor magnus, biceps femoris (long head), semimembranosus, semitendinosus, and adductor longus, tended to have lower IVIM D values in OPMD than in controls, whereas less fat-infiltrated muscles showed smaller or non-significant differences. This suggests that reduced IVIM D is more closely seen in muscles with greater disease FF involvement.

Figure 9: Relationship between FF and IVIM f across thigh muscles in OPMD, overall and by disease duration: Each point represents a muscle-level measurement, colored by muscle. Overall, FF showed a weak positive correlation with IVIM F (Spearman $\rho = 0.28$). Figure 7B represents: Spearman correlation coefficients with 95% confidence intervals for the association between FF and IVIM F, stratified by disease-duration period (0–5, 5–10, 10–15, and 15+ years). Correlations were corrected within each duration bin using the FDR-BH. The results show that the relationship between FF and IVIM f varies by muscle and disease stage, and that association strength between FF and IVIM f might indicate stages of disease activity.

Figure 10: No significant differences between OPMD participants and controls when assessing with IVIM F Each point represents an individual muscle measurement, with left and right sides averaged for each muscle. Comparisons were performed using unpaired Wilcoxon tests for each muscle, with (FDR-BH) correction applied across thigh muscles. P values displayed above each muscle correspond to BH-FDR-adjusted values; ** indicates BH-FDR $p < 0.05$. Overall, IVIM f values showed substantial overlap between OPMD and control muscles, with no consistent significant differences after correction.

Figure 11: Association between thigh muscle fat fraction and IVIM D* in OPMD. The left panel shows the relationship between FF and IVIM D* across 12 thigh muscles in participants with OPMD, using left-right averaged values for each muscle. Each point represents one muscle-level observation and is color-coded by muscle. The pooled Spearman correlation coefficient is shown on the plot. The right panel summarizes, for each muscle, the mean FF ± SD together with the muscle-specific Spearman correlation coefficient and Bonferroni-

adjusted p value for the association between FF and IVIM D*. Muscles are presented in descending order of mean FF.

Figure 12: Comparison of thigh IVIM D* between OPMD and controls. Boxplots show left-right averaged IVIM D* values for 12 thigh muscles in participants with OPMD and controls. Individual subject values are overlaid as jittered points. For each muscle, groups were compared using unpaired Wilcoxon rank-sum tests, and p values are shown above the corresponding muscle. FDR-BH was applied within the thigh muscle set; ** indicates BH-FDR-adjusted $p < 0.05$. Overall, most muscles showed no differences between the two groups.

Figure 13: Correlation between FF and T2 relaxation time: Figure 13A showing the association between FF and T2 relaxation time across thigh muscles in patients with OPMD. Each point represents a muscle-level measurement. Overall, FF and T2 showed a weak positive trend (Spearman $\rho = 0.18$). 13B represents: Individual muscle summary of mean FF, Spearman correlation coefficients, and Bonferroni-corrected p values for the association between FF and T2 in individual thigh muscles. Correlations were generally weak and heterogeneous across muscles, with no robust associations remaining after Bonferroni correction, although nominal positive trends were seen in selected muscles such as the sartorius, the adductor longus, the vastus medialis, and the vastus lateralis. These findings suggest that the relationship between fat replacement and T2 relaxation time is variable across thigh muscles in OPMD at a cross-sectional level and more needs to be assessed with a longitudinal timepoint.

Figure 14: Difference between OPMD participants and controls on T2 relaxation time. Each point represents an individual muscle measurement, with left and right sides averaged for each muscle. Comparisons were performed using unpaired Wilcoxon tests for each muscle, with (FDR-BH) correction applied across thigh muscles. P values displayed above each muscle correspond to BH-FDR-adjusted values; ** indicates BH-FDR $p < 0.05$. Overall, T2 values showed no significant differences between OPMD group and controls, although semitendinosus showed a nominal difference at the raw p-value level. These findings suggest that T2 relaxation time does not clearly distinguish OPMD from controls across most thigh muscles in this cohort.

Figure 15. Mean FF across disease-duration bins in lower-body and upper/trunk muscle regions. Violin plots show the distribution of subject-level mean FF values across disease-duration bins (0–5, 5–10, 10–15, and ≥15

years) for the lower body and upper/trunk regions. Within each violin, the boxplot summarizes the interquartile range and median, individual points represent subjects, and the white diamond denotes the group mean. The grey horizontal band represents the control interquartile range (IQR), and the dashed horizontal line within that band indicates the control median. Adjacent-bin unpaired Wilcoxon rank-sum tests with BH-FDR correction were performed separately within each region, with adjusted p values shown above the brackets and an * indicating statistical significance. In the lower body, FF was significantly higher in the 5–10-year group compared with the 0–5-year group, whereas later adjacent comparisons were not significant.

Figure 16: Correlations between FF and disease duration for the 10 most fat-affected muscles Scatter plots show FF versus disease duration for the 10 muscles with the highest mean FF. Points are colored by disease-duration s (0–5, 5–10, 10–15, ≥15 years). The locally estimated scatterplot smoothing line represents the trend. Each panel reports the Spearman correlation (ρ) between duration and FF with Bonferroni-corrected p-values. TFF generally increases with longer disease duration, with several muscles demonstrating significant monotonic correlations after Bonferroni correction.

Figure 17: Mean composite ADC values decrease with disease duration. Violin plots show the distribution of subject-level mean ADC values across disease-duration bins (0–5, 5–10, 10–15, and ≥15 years) for the lower body and upper/trunk regions. Within each violin, the boxplot summarizes the interquartile range and median, individual points represent subjects, and the white diamond denotes the group mean. The grey horizontal band represents the control interquartile range (IQR), and the dashed horizontal line within that band indicates the control median. Adjacent-bin unpaired Wilcoxon rank-sum tests with BH-FDR correction were performed separately within each region, with adjusted p values shown above the brackets. No adjacent-bin comparisons were significant in either region, indicating that mean ADC did not show a clear stepwise change and could be prone to more muscle specific variabilities across disease-duration period.

Figure 18: Correlation between Diffusivity decreases and disease duration for the 10 most fat affected muscles. Scatter plots show disease duration years versus ADC for the 10 muscles with the highest mean FF. Each point represents one participant and is color-coded by duration strata (0–5, 5–10, 10–15, ≥15 years). The locally estimated scatterplot smoothing line represents the trend. Spearman's ρ and Bonferroni-corrected p-values

(across the 10 muscles) are displayed within each panel. ADC generally decreases as disease duration increases, consistent with reduced diffusivity in more advanced disease.

Supplemental Figure 1: Muscle MRI acquisition protocol and segmentation workflow.

Supplemental Figure 2: Whole body correlation between FF-ADC. High Fat Fraction muscles in the thigh, pelvic and calf region have a stronger negative correlation with ADC.

Supplemental Figure 3: Sentinel muscle selection and preliminary control sample size estimation**.** (A) The five thigh muscles with the highest mean FF in OPMD were identified. For each muscle, the table shows the mean fat fraction, standard deviation, and range in OPMD. (B) The same sentinel muscles are shown in controls, with corresponding mean fat fraction, standard deviation, and range. Across all five muscles, FF was lower in controls than in OPMD participants. (C) A participant-level sentinel muscle fat fraction was calculated as the mean across these five muscles. This summary table shows the observed OPMD and control sample sizes, the mean sentinel muscle FF in each group, and the standardized effect sizes (Cohen's d and Hedges' g) derived from the group difference.

List of Tables

Chapter 1: Introduction

Oculopharyngeal muscular dystrophy (OPMD; OMIM 164300) is a late-onset, progressive muscular dystrophy characterized by ptosis (drooping eyelids), dysphagia (trouble swallowing), and proximal limb weakness [1,2]. OPMD prevalence is higher in certain geographic regions and ethnic groups, largely because of founder effects [3–6]. In Canada, OPMD is particularly common in French Canadians, with a reported prevalence of 1/1,000 versus 1/200,000 worldwide [7]. The disease results from a (GCN) trinucleotide repeat expansion in exon 1 of the *Polyadenylate-binding protein nuclear 1* (*PABPN1*) gene [1]. Diagnosis relies on the characteristic clinical phenotype [9] and is confirmed by genetic testing demonstrating a heterozygous expanded allele (11–18 repeats) or, less commonly, biallelic expansions (homozygous or compound heterozygous) or point mutations [10].

Limitations of clinical outcome measures

In many muscular dystrophies (MD), clinical outcome measures evaluate the overall function of composite muscle groups rather than function of individual muscles and are often limited to patients with preserved residual muscle function and cannot assess patients with more advanced disease [11]. In OPMD, many commonly used outcome measures including the muscle strength testing and clinical functional assessments (*e.g.,* the 6-minute walk test), lack sensitivity to detect disease progression in the context of slowly progressive disorder [2,9,12]. Clinical outcome measures such as manual muscle testing, functional walking assessments, swallowing-related assessments, and quality-of-life measures may not always detect small changes in muscle over shorter follow-up periods [12]. In addition, clinical measures can also be affected by factors such as patient effort, fatigue, motivation, and examiner variability [13–15]. In addition to the high cost of clinical trials, in rare diseases such as OPMD, appropriate follow-up periods and large sample sizes may be difficult to achieve, highlighting the need for sensitive biomarkers in natural history studies and future therapeutic trials [11,12,16]. In OPMD, a participant may have measurable fat replacement or tissue change in specific muscles on MRI before this produces a change in a global clinical score [41]. Therefore, imaging biomarkers that assess the pattern of involvement in muscles may prove to be important for diagnosis and as a biomarker to assess disease progression in future clinical trials [11,39–43]. This is especially relevant as disease-modifying approaches for OPMD are being developed, including RNA-based and gene-directed therapeutic strategies [17,18]. For these reasons, there is a

need for objective and reproducible biomarkers that can assess disease severity, identify muscles involved early, and quantify progression at the individual-muscle level.

MRI as a biomarker in muscular dystrophies

Muscle MRI is an emerging biomarker in MD to assess the pattern of affected muscles and severity of muscle involvement [11,26]. Conventional muscle MRI can be assessed qualitatively to identify fatty replacement, edema/inflammation signal changes, muscle atrophy, and selective patterns of involvement [11,33,34]. These findings can help in diagnosis and disease classification [11,26,34]. In addition to qualitative assessment of affected muscles, quantitative MRI (qMRI) provides quantitative values that can be compared across muscles, participants, and longitudinal time points, and can provide more objective measure and can be more reliable than qualitative assessment tools [11,21,26,34].

qMRI is useful in MD to detect structural muscle changes in the muscle, particularly fat replacement and monitor progression over time that may not be captured by functional measures. Longitudinal MRI studies in MD have shown progression over time and support MRI as a sensitive outcome measure for clinical trials [19,21,23,24]. Sample-size modelling has suggested that approximately five times more participants may be required when using 6-minute walk distance compared with MRI biomarkers, further supporting qMRI as a sensitive trial endpoint [20]. In a qMRI gene-therapy study in Duchenne MD, the treated group showed 1.01 percentage points less progression in soleus muscle than placebo [19,25]. In limb-girdle MD and facioscapulohumeral muscular dystrophy, quantitative MRI has also been used to monitor fat replacement and disease progression over time [21,23,27].

qMRI provides continuous and objective measurements of muscle composition. Quantitative measures may improve reproducibility and reduce observer dependence, which is important for multicentre studies and clinical trials [11,26,43]. qMRI can also assess specific muscles, muscle groups, or whole-body patterns of disease involvement. In OPMD, previous MRI studies have shown selective muscle involvement with tongue, adductor magnus, biceps femoris long head and muscles of the proximal pelvis commonly identified among the muscles

with the most fat fraction (FF) [39–43]. Individual muscles assessment aided by qMRI may therefore help identify affected and relatively spared muscles and may support monitoring of disease severity and progression [39-43]

Several MRI-derived variables can be used to assess different aspects of muscle pathology. FF, usually derived from Dixon-based techniques, reflects chronic fatty replacement of muscle [22,26,31]. T2 relaxation time and water-sensitive measures may reflect increased free water, edema-like change, or active tissue injury [28,34–36]. Diffusion-weighted measures, including apparent diffusion coefficient (ADC) and intravoxel incoherent motion parameters (IVIM), may provide information about water motion, tissue microstructure, and perfusion-related effects [37,38].

Fat fraction/Dixon imaging in muscular dystrophy

Fat replacement is one of the main pathological findings assessed by muscle MRI in muscular dystrophy. In this process, normal contractile muscle tissue is progressively replaced by fat and connective tissue, reflecting chronic structural damage [26,28–31]. Fat replacement represents a more advanced and less reversible form of muscle injury, FF has become one of the most widely used quantitative MRI biomarkers in muscular dystrophy [26,31,39,40].

Dixon-based MRI techniques assess separate fat and water signal and allow generation of FF maps [22,26,31]. These maps provide a numerical estimate of the proportion of fat to the combined fat and water signal within a voxel or muscle, allowing the degree of fatty replacement to be quantified [22,26,31]. This is useful in muscular dystrophy because degree of FF varies in different muscles and may progress at different rates across the body [19,21,23,26,27]. FF has been used to monitor chronic muscle involvement over time, including in Duchenne MD, limb-girdle MD, and facioscapulohumeral muscular dystrophy and OPMD [19,21–23,25,27]. These studies support FF as a structural biomarker of disease severity and progression, particularly in conditions where clinical change may be slow or where different muscles are affected to different degrees [11,19,21,23,26].

In OPMD, FF has been one of the main imaging markers studied so far. Prior MRI studies have shown a selective pattern of fat replacement, with the tongue, adductor magnus, hamstrings, and soleus frequently identified among the most affected muscles [39,40,42,43]. These findings suggest that FF could characterise both the severity

and pattern of muscle involvement in OPMD. However, FF mainly reflects chronic structural replacement and may not fully capture earlier or more active tissue changes. Therefore, this thesis intends to assess FF together with ADC, IVIM-derived parameters, and T2 relaxation time to determine whether water-based qMRI measures show earlier sings of disease activity before chronic fat replacement in OPMD.

Water-sensitive MRI measures and T2 mapping in muscle disease

In addition to fat replacement, muscle MRI can assess water-related signal abnormalities. Increased water signal in muscle can reflect edema-like change, tissue injury, inflammation, sarcolemma leakiness, or necrosis [28,33,35]. In muscular dystrophy, edema-like changes may occur before or alongside fat replacement, although the relationship between edema and later fat replacement can vary depending on the disease and muscle involved [28,33]. Therefore, water-sensitive imaging may provide information that is complementary to FF.

Conventional fat-suppressed T2-weighted or Short T1 Inversion Recovery imaging can show edema-like signal changes qualitatively [33,35]. However, qualitative assessment is limited because it depends on visual interpretation and may not provide a precise numerical measure [34,35]. T2 mapping allows quantitative assessment of T2 relaxation time and provides a numerical value that reflects water-related tissue properties [34,35]. Higher T2 relaxation times are generally associated with increased muscle water content and may be seen in edema, inflammation, or muscle injury [34–36].

In inflammatory myopathies, qMRI measures including T2 mapping have been correlated with histopathological findings, supporting the biological relevance of water-sensitive MRI measures in active muscle disease [28,34,35,36]. T2 mapping has also been studied at a preliminary level in OPMD. In a small, longitudinal, quantitative MRI study, 8 patients with OPMD and 5 healthy controls were examined twice at an interval of 13 months. MRI included 2-point Dixon for fat fraction and a multi-contrast turbo spin echo sequence to calculate quantitative T2 values. Over the study period, motor function measurements and visual scores showed no significant change, while overall T2 values increased from 49.4 to 51.6 ms and muscle FF increased from 19.2% to 20.7% in patients, with no increase in controls [41]. This suggests that qMRI may detect subclinical progression in OPMD when semiquantitative scores and motor function measures remain unchanged [41].

DWI/ADC and IVIM in muscle disease

Diffusion-weighted imaging (DWI) is an MRI technique that measures the motion of water molecules within tissue and can provide information about tissue microstructure [38,49]. The Apparent Diffusion Coefficient (ADC) is derived from diffusion-weighted imaging and provides a quantitative measure of water diffusion within tissue [38]. In skeletal muscle, ADC may be influenced by tissue structure, extracellular space, fibre organization, edema-like change, fat replacement, muscle type, and acquisition-related factors such as the b-values. The b-value is a diffusion sensitizing parameter in diffusion-weighted magnetic resonance imaging that characterterizes the strength and timing of the applied diffusion encoding gradients. It determines the extent to which the MR signal is attenuated by the random (Brownian) motion of water molecule and is expressed in s/mm^2 used for calculation [37,38,49,58,66]. In muscle disease, altered water diffusion may reflect changes in tissue organization and disease activity. Increased water content or inflammatory change may increase diffusivity, while fibrosis, fat replacement, or reduced extracellular water space may reduce measured diffusion [37,38,58]. This may indicate that ADC values are influenced by disease stage and the predominant muscle pathology, reflecting variable contribution from edema, inflammation, fibrosis, and fatty infiltration.

Intra-Voxel incoherent imaging uses multiple b-values to separate tissue diffusion from perfusion-related microcirculatory motion [37]. IVIM produces three main parameters: diffusion coefficient (IVIM D), pseudo-diffusion coefficient (IVIM D*), and perfusion fraction (IVIM F). The IVIM D reflects tissue diffusion after reducing the influence of perfusion-related motion. The IVIM D* represents the pseudo-diffusion coefficient associated with microvascular flow, and perfusion fraction reflects the relative signal contribution from the perfusion related compartment [37]. IVIM can assess both diffusion and perfusion-related components without contrast administration [37]. In MD, IVIM may be useful because muscle pathology can involve both structural tissue changes and changes in microvascular perfusion [37]. A study reported that thigh muscle IVIM and T2 mapping parameters differed between autoimmune myositis and muscular dystrophy, with IVIM parameters showing diagnostic value [56]. In that study, ADC, IVIM D, IVIM F, and T2 relaxation time were significantly different between autoimmune myositis and muscular dystrophy groups, while pseudo-diffusivity did not differ significantly [56]. These findings could indicate that diffusion and perfusion-related MRI measures may provide information about muscle pathology in addition to fat replacement.

In OPMD, the role of ADC and IVIM has not been well studied. Previous OPMD imaging studies have focused mainly on fat replacement, muscle pattern recognition, and longitudinal FF progression [39–43]. Moreover, no OPMD-related studies have assessed the relationship between FF and water-based MRI measures such as ADC, IVIM-derived parameters, and T2 relaxation time. Therefore, assessing these measures in relation to FF and disease duration may help determine whether water-based and diffusion-based qMRI measures reflect changes in muscle tissue characteristics before or alongside fat infiltration in OPMD.

Prior OPMD MRI literature

Previous MRI studies in OPMD have shown that muscle involvement follows a selective pattern rather than a uniform whole-body distribution in the early disease duration periods. A large cross-sectional study of 168 genetically confirmed OPMD patients showed fatty replacement in 96.7% of symptomatic patients, with the tongue, adductor magnus, and soleus identified as the most affected muscles [39]. Muscle involvement on MRI also correlated with disease duration and functional impairment, supporting MRI as a useful method to define disease pattern and severity in OPMD [39].

Early-stage OPMD studies have shown that the pelvic girdle and the proximal leg involvement can occur relatively early in the disease course. In one study, patients with early OPMD showed higher fat replacement in the hip adductors and hamstrings than controls, and this involvement was associated with impaired daily life activities [42]. Longitudinal MRI studies have further supported the role of qMRI in OPMD. A longitudinal study with a sample size of 43 patients found that the tongue, adductor magnus, and soleus had the highest fat infiltration levels, and that overall FF increased by 3.8% over 20 months [40]. The study also showed that progression of fat replacement in affected muscles correlated with clinical severity, supporting FF as a biomarker of disease progression in OPMD [40].

A smaller longitudinal quantitative MRI study showed that motor function measurements and semi quantitative scores did not change significantly over 13 months, while qMRI measures changed over the same period. This suggest that qMRI may detect subclinical progression in OPMD when other measures are less sensitive [41].

qMRI may also improve reliability compared with qualitative or semiquantitative MRI assessment [43]. A study reported higher inter-rater agreement for quantitative measures than for semiquantitative scoring, further supporting qMRI as an outcome measure in OPMD [43]. Overall, previous OPMD MRI studies have assessed FF as an important marker of disease involvement and progression. However, the relationship between FF, ADC, IVIM parameters, and T2 relaxation time has not yet been evaluated in OPMD [39–43].

Knowledge gap and thesis rationale

Despite the growing use of muscle MRI in MD, important gaps remain in OPMD imaging. Previous studies have shown that FF can identify disease-specific patterns of fat replacement and detect progression over time [39–43]. However, these studies have been limited by small sample sizes, short follow-up periods, limited numbers of muscles analysed, and the absence of several water-based MRI measures such as ADC, IVIM, and T2 relaxation time in OPMD [39–43]. Moreover, there are currently no OPMD-related studies that have assessed and correlated water-based MRI measures such as ADC, IVIM-derived parameters, and T2 relaxation time with FF.

Further investigation is therefore needed to assess whether water-based and diffusion-based MRI measures provide earlier signs of disease activity in OPMD. The Ottawa Neuromuscular Imaging group has previously assessed imaging in OPMD and other neuromuscular disorders [43–45]. This thesis evaluates whole-body qMRI in OPMD by assessing the relationship between FF and water-based MRI measures.

Research Hypotheses and Objectives

Hypothesis

The hypothesize was that MRI water measures, including ADC, IVIM parameters, and T2 relaxation time, can detect changes in tissue characteristics of muscle and may detect edema before fat infiltration, and that the pattern of muscles involvement on qMRI differs between OPMD participants and controls.

Aim 1

To quantify, cross-sectionally, the correlation between FF and water-based qMRI measures, including ADC, IVIM D, IVIM F, IVIM D*, and T2 relaxation time. FF–ADC correlations will be assessed across 97 muscles, while FF–IVIM and FF–T2 relaxation time correlations will be assessed across 24 thigh muscles.

Aim 2

To determine whether mean FF increases and ADC changes across disease-duration periods relative to the control reference range, as an indirect cross-sectional assessment of disease progression.

Aim 3

To assess the association between MRI measures and disease duration with respect to FF and ADC in individual muscles, while comparing findings with controls.

Chapter 2: Methods

Study design

We performed a cross-sectional qMRI study of participants with genetically confirmed OPMD. The study was designed to assess the pattern of muscle involvement on whole body qMRI and to examine the relationship between FF and water based qMRI biomarkers including ADC, IVIM, T2 relaxation time. In addition to comparing imaging measures between OPMD participant and control, the aim was to assess whether water-related parameters might detect disease related muscles changes earlier than fat replacement.

Study Ethics

This study was conducted at The Ottawa Hospital in Canada with participants recruitment through the Neuromuscular Centre. Research Ethics Board approval was obtained for participants with OPMD as part of a large neuromuscular disease cohort assessing imaging and biomarkers (REB # CTO 1590) as well as controls (REB# OHRI 4285). Written informed consent was obtained from all participants prior to enrollment.

OPMD participants

The study population consisted of patients with genetically confirmed OPMD. Participants with OPMD were recruited through the Neuromuscular Centre at The Ottawa Hospital, Ottawa, Canada.

Control group

The control group comprised of patients referred for myalgias and/or mild hyperCKemia with a negative family history of OPMD. Controls were included only if they did not meet diagnostic criteria for any known neuromuscular disorder on clinical assessment, genetic testing and, when available, electromyographic evaluation.

Sample size estimation for OPMD participants

An a priori sample size calculation was conducted using G*Power (version 3.1) (Exact test family; correlation: bivariate normal model, two-tailed) [81]. The calculation was based on Aim 1 cross sectional analysis which examined the association between FF and water-based MRI measures, particularly ADC and IVIM D in the OPMD group. Assuming an expected correlation coefficient of $\rho = 0.50$, with the null hypothesis set at $\rho = 0$, a

two-sided significance level of 0.05, and statistical power of 0.80, the estimated required total sample size was 29 participants with OPMD.

Observed effect size for preliminary estimation of controls

As a preliminary approach to estimate the sample size for controls, effect sizes were quantified using standardized mean differences based on participant-level sentinel muscle FF. Sentinel muscles were defined as the five thigh muscles with the highest mean FF in OPMD. Left and right sides were averaged for each muscle, and the mean across the selected sentinel muscles was calculated for each participant. The observed sentinel muscle FF in 40 participants with OPMD and 12 controls, was 30.7 ± 19.9% in OPMD and 11.0 ± 5.6% in controls. Cohen's d expressed the difference between OPMD, and control means in units of the pooled standard deviation, whereas Hedges' g provided a small-sample bias-corrected estimate the corresponding effect sizes were d = 1.111 and g = 1.094. This observed effect size was then used to estimate the control sample size required to achieve 80% power at a two-sided significance level of 0.05 [74,75]. Under equal allocation, 14 participants per group were estimated to be required, corresponding to 8 controls when the OPMD sample size was fixed. Effect size magnitude was interpreted using conventional thresholds, with values of approximately 0.2, 0.5, and 0.8 corresponding to small, medium, and large effects, respectively [76].

Inclusion and exclusion criteria

Patients were included in the OPMD group if they had genetically confirmed OPMD and had completed whole-body muscle qMRI. A subgroup of participants also underwent an extended qMRI protocol including apparent diffusion coefficient (ADC), intravoxel incoherent motion (IVIM), and T2 mapping sequences. Exclusion criteria were age below 18 years, pregnancy, and contraindications to MRI.

Clinical assessment and chart review

Muscle strength was graded using Medical Research Council (MRC) grading scale [72]. Bilateral strength assessment included shoulder abduction, shoulder external rotation, elbow flexion, elbow extension, hip flexion, hip abduction, and hip adduction with a total score of 70. All participants underwent chart review for assessing

weakness with MRC scale, age at symptom onset, medication review, creatine kinase (CK) levels, genetic test, and clinical examination by a neurologist (JWC) with 10 years of experience in assessing NMDs.

MRI acquisition

MRI was performed at 3 Tesla (Magneton Prisma Fit, Siemens Healthineers, Erlangen, Germany). A head coil, two body matrix coils, a peripheral leg coil and the table built-in spine coil were used for signal detection. Each participant was examined in head-first, supine position. The protocol consists of a Fast View localizer sequence (time = 33 s) followed by a clinical and quantitative imaging protocol consisting of a 3D volumetric interpolated breath-hold examination (VIBE) in- and opposite phase sequence (2-point Dixon), and an axial whole body diffusion sequence covering proximal from at least the nose level at head to the distal aspect of the soleus. Additionally, an intravoxel incoherent motion (IVIM) and a T2 mapping sequence were performed on the thighs of the study participants. The total imaging time (including the localizer) was 30 min 21 sec. (The protocol parameters in the **Appendix/Supplementary table 1**; the protocol also included a 6-point Dixon sequence that was not evaluated in this thesis). With table/bed movements and pre-scans (for frequency measurement, pulse calibration and shimming) the MRI session time was 40 min. All participants had the 2-point Dixon sequences, a subset of them had the additional MRI protocol including (ADC, IVIM, T2 mapping). Quantitative MRI maps were generated for each sequence. FF maps were computed from the water-only and fat-only images of the 2-point Dixon dataset. ADC maps were derived from diffusion dataset acquired at b = 50 s/mm² and b = 800 s/mm². For IVIM processing, diffusion-weighted images acquired with b-values ranging from 0 to 1000 s/mm² were used to derive the quantitative diffusion (D), pseudo diffusion (D*) and perfusion fraction (f) maps. Images acquired with six echo times were used to generate quantitative T2 maps.

Downloading images from PACS

For each subject, imaging data were downloaded in DICOM format from the Picture Archiving and Communication System (PACS) at The Ottawa Hospital. Following image retrieval, each participant was assigned a unique study identification number to ensure de-identification of personal health information. For the 2-point Dixon sequence, the in-phase, opposed-phase, fat, and water images were downloaded together.

For the ADC sequence, the b = 50 s/mm² and b = 800 s/mm² images were also downloaded together. For IVIM, each diffusion b-value dataset (from b = 0 s/mm² to b = 1000 s/mm²) was exported as a separate DICOM series. Similarly, for the T2 mapping sequence, each of the six echo-time images was saved as an individual DICOM series. This organization was required for subsequent post-processing and generation of quantitative IVIM parameter maps and T2 maps using MATLAB-based routines developed by the Neuromuscular Imaging research team.

Data acquisition and post map processing through MATLAB

For the 2-point Dixon sequence, parametric maps were directly available from PACS. The segmented region of interest (ROI) was propagated to the corresponding FF map within ITK-SNAP, enabling extraction of quantitative values.

A similar approach was applied for ADC. ROIs defined on the diffusion-weighted image (b = 50 s/mm²) were propagated to the corresponding ADC map, which was calculated from the b = 50 and b = 800 s/mm² datasets and obtained directly from PACS.

IVIM parametric maps were reconstructed from the raw diffusion-weighted data using in-house developed software implemented in MATLAB (version R2021a). IVIM fitting was performed following using a segmented least-squares method [77]. Briefly, a b-value threshold of 200 s/mm² was applied to first estimate the slow diffusion coefficient (D) from higher b-values, minimizing perfusion-related effects. Subsequently, the perfusion fraction (f) and pseudo-diffusion coefficient (D*) were estimated using the full b-value range. Quantitative IVIM parameters were then extracted from the propagated ROIs.

T2 mapping was performed from multi-echo spin-echo data using the open-source MyoQMRI framework [78,79]. Signal evolution across echo times was modeled using an extended phase graph (EPG) formalism to account for stimulated echoes and refocusing flip angle deviations. Voxel-wise T2 values were estimated by fitting the measured signal decay to the EPG-based model. The resulting T2 maps were then used for quantitative analysis, with ROIs propagated to the corresponding maps to extract mean T2 values.

Segmentation with ITK-SNAP

Manual muscle segmentation was performed using ITK-SNAP version 3.8.0. For the 2-point Dixon and ADC datasets, 97 muscles were segmented across 7 anatomical levels to provide comprehensive whole-body muscle coverage (**Supplementary Figure 1**). This broad assessment was used to characterize the disease-specific pattern of muscle involvement, identify relatively spared and preferentially affected muscles, and evaluate muscles that may be difficult to assess reliably on clinical examination [44–46]. As an exploratory analysis, 24 thigh muscles were additionally segmented on the IVIM and T2 relaxation time datasets.

Single-slice segmentation was performed at predefined anatomical landmarks. These included the tongue at the lower border of the second cervical vertebra, shoulder muscles at the level of the second thoracic vertebra, paraspinal muscles at the level of the third lumbar vertebra, upper pelvis at the level of the anterior inferior iliac spine, lower pelvis at the level of the pubic symphysis, thigh at the mid-level below the origin of the ischiotibial tendon, and calf below the tibial plateaus.

For the 2-point Dixon sequence, manual segmentation was performed on the in-phase images and verified using the opposed-phase images and corresponding FF maps. Because Cartesian MRI is susceptible to chemical-shift artifact in the readout direction, this was assessed across the in-phase, opposed-phase, and FF datasets, and segmentation margins were adjusted accordingly. For IVIM, segmentation was performed on the lowest b-value image (b = 0 s/mm²). For ADC, segmentation was performed on the b=50 s/mm² dataset. For T2 mapping, segmentation was performed on the image acquired at the shortest echo time, which provided the highest signal-to-noise ratio and optimal contrast. After segmentation, all segmentation levels were reviewed with Dr. Marcos Sampaio, musculoskeletal radiologist at The Ottawa Hospital.

For diffusion-weighted imaging datasets, including ADC and IVIM, segmentation was assessed with the corresponding 2-point Dixon images from the same participant as an anatomical reference to identify the boundaries of muscles that were difficult to delineate in instances of low signal to noise ratio. This also allowed cross-referencing of the correct anatomical level and helped identify any motion or positional shift that may have occurred between sequences during the whole-body MRI acquisition.

Data analysis and statistics

Statistical analyses were performed using R version 4.5.2 (2025-10-31) and GraphPad Prism version 10.6.1. The strength of association for Spearman correlation coefficients was interpreted as negligible (0.00–0.10), weak (0.10–0.39), moderate (0.40–0.69), strong (0.70–0.89), and very strong (0.90–1.00) [47]. To account for multiple comparisons, both Bonferroni correction and false discovery rate adjustment using the Benjamini–Hochberg method (FDR-BH) was applied across the set of muscles tested within each analysis. Statistical significance was interpreted according to the multiple-comparison correction applied within each analysis. For all statistical tests, a p-value < 0.05 was considered statistically significant

MRC scores were compared between the OPMD and control groups using the nonparametric Kruskal–Wallis test. Whole-body FF was visualized using a heatmap in which left and right muscle values were averaged within each participant. Participants were arranged on the y-axis according to time since symptom onset, while muscles were arranged on the x-axis in descending order of overall mean FF to illustrate the range and pattern of fat replacement.

Spearman's rank correlation was used to assess the association between muscle FF, ADC, IVIM parameters, and T2 relaxation time. For each muscle and sequence, left and right values were averaged per participant. A 95% confidence interval for each correlation coefficient was calculated using Fisher's z-transformation, and p-values were adjusted for multiple comparisons using Bonferroni correction.

Differences in FF, ADC, IVIM, and T2 relaxation time between OPMD participants and controls were assessed for each muscle using the unpaired Wilcoxon rank-sum test. Raw and FDR-BH-corrected p-values were reported.

Muscles for duration-based analyses (correlating with length of time with disease symptoms) were selected according to the highest mean FF in the OPMD group. For each selected muscle, Spearman's rank correlation was computed between disease duration and FF or ADC, and p-values were Bonferroni-corrected across the 10 muscles tested. Potential non-linear associations between disease duration and ADC were explored using locally weighted regression (LOESS) smoothing [73]. LOESS fits locally weighted polynomial regressions across neighborhoods of the predictor variable, allowing flexible modeling of trends without assuming a global linear

relationship. The resulting smoothed curves were overlaid on scatterplots and generated in R using the ggplot2 package with geom_smooth (method = "loess", se = FALSE) and default settings (span ≈ 0.75; degree = 2). This analysis was performed for descriptive visualization only and did not replace the primary inference based on Spearman correlation.

To assess whether ADC measures showed earlier signs of disease activity, participants were stratified into four exploratory clinical categories (“bins”), based on time since reported symptom onset: 0–5 years, 5–10 years, 10–15 years, and >15 years. For each participant, qMRI values across individual muscles were averaged to generate regional mean FF and ADC values. Differences between adjacent duration bins were assessed using unpaired Wilcoxon rank-sum tests (Mann–Whitney U), with FDR-BH correction applied for multiple comparisons.

Chapter 3: Results

Patient demographics

Table 1 summarizes the demographics of the participants. Fifty-two participants were recruited for this study, 40 patients with OPMD and 12 controls. Within OPMD participants, 22 were female and 18 were male, with a mean age at MRI 61.6 ±10.8 years. 12 controls were included, 5 females and 7 males with mean age at MRI of 43.1±15.1 years. All 40 participants with OPMD had the 2-point Dixon for FF mapping, 37 had the scans for ADC (whole body) and IVIM (thigh) and 35 had T2 mapping (thigh). All 12 controls had whole body 2-point Dixon, 9 had IVIM (thigh) and 8 had ADC (whole body) and T2 mapping (thigh). All the scans were completed between Feb 2023 and Jan 2025.

In MRC strength testing, the OPMD group had lower overall strength than controls, with a mean MRC score of 67.3 ± 3.2 compared with 70.0 in controls. The relationship between this overall strength score and regional qMRI measures was derived from grouped muscles of the calf, pelvis, thigh, and upper body/face (Supplemental Table 3). FF showed strong to moderate negative correlations with MRC score with the calf (ρ = -0.74), pelvis (ρ = -0.67), thigh (ρ = -0.65), and upper body/face (ρ = -0.54) muscles, indicating that higher FF was associated with lower overall muscle strength score. ADC showed moderate positive correlations with MRC score in the calf (ρ = 0.51), pelvis (ρ = 0.56), and thigh (ρ = 0.48) muscles, indicating that the strength was higher in muscles with low FF and normal diffusivity, while IVIM D and IVIM D* in the thigh also showed moderate positive correlations (ρ = 0.46 and ρ = 0.41, respectively). In contrast, IVIM f showed a weak negative correlation (ρ = -0.19) and T2 relaxation time showed a weak positive correlation (ρ = 0.21), neither of which was significant after Bonferroni correction.

Table 1: Study participants demographics and MRC score

Group	N Female/Male	Age at MRI (years) (Mean ± SD; Range)	Years of Disease at MRI (Mean ± SD; Range)	MRC Muscle Power Score (Mean ± SD; Range)
OPMD	40 (22/18)	61.6 ±10.8; 40.0-85.0	10.9±7.1;0-32.8	67.3 ± 3.2; 56.0 -70.0*
Control	12 (5/7)	43.5 ±14.4; 18.0-63.0	N/A	70.0 ± 0.0; 0

Oculopharyngeal muscular dystrophy (39 patients were heterozygous with 13 GCN repeats, 1 patient with 16 repeats in *PABPN1*) MRC: Medical Research Council * indicates significant p value <0.05 vs controls

Sex based variation in relation to age and disease duration

Male participants with OPMD were slightly older than female participants as highlighted in **Figure 1**, although the difference in age at MRI was not statistically significant. In contrast, disease duration was longer in males than in females and reached statistical significance. The summary tables show that females had a mean age of 59.23 years and a mean disease duration of 8.9 years, whereas males had a mean age of 64.61 years and a mean disease duration of 12.99 years.

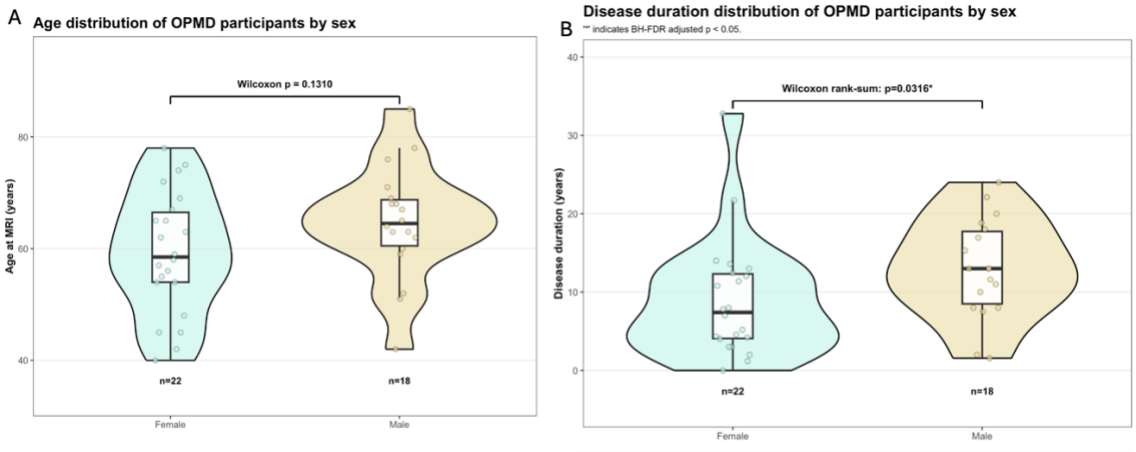

Age summary by sex

	n	Mean age	SD	Median	Min	Max
Female	22	59.23	10.94	58.50	40.00	78.00
Male	18	64.61	10.10	64.50	42.00	85.00

Disease duration summary by sex

	n	Mean duration	SD	Median	Min	Max
Female	22	8.91	7.53	7.40	0.00	32.77
Male	18	12.99	6.32	13.00	1.56	24.00

Figure 1: Age and disease duration distribution by sex in OPMD. (A) Violin plots with overlaid boxplots and individual data points show age at MRI in female and male participants with OPMD. (B) Violin plots with overlaid boxplots and individual data points show disease duration in female and male participants with OPMD. P values indicate Wilcoxon rank-sum comparisons between sexes. Tables below each panel summarize number of

participants, mean, standard deviation, median, minimum, and maximum values for age and disease duration by sex.

Pattern and range of fat fraction at a cross-sectional level

In participants with OPMD, FF per muscle ranged from highly affected muscles such as adductor magnus (FF=41.0 ± 28.9 %) to 'mostly spared' muscles such as rectus femoris (FF=5.8 ±3.0 %). **Figure 2** shows an FF heatmap of all analyzed muscles. With participant sorted by time since self-reported symptom of ptosis and dysphagia to qMRI on the y axis. The muscles with highest FF in the OPMD cohort were the adductor magnus (FF = 41.2 ± 28.9 %), the soleus (FF = 39.2 ± 25.9 %), the tongue (FF = 38.9 ± 20.3 %), the gluteus maximus (FF = 37.9 ± 23.2 %) and biceps femoris long head (FF = 33.8 ± 25.2 %). Rectus femoris and vastus lateralis were amongst the least fat replaced in the thigh compartment (FF = 5.8 ± 3.0 %, FF = 8.1 ± 2.6 %). Furthermore, the heatmap indicates that the muscles that are most fat replaced are also affected earlier in the disease course, and that the FF pattern could be variable among participants in these high FF muscles.

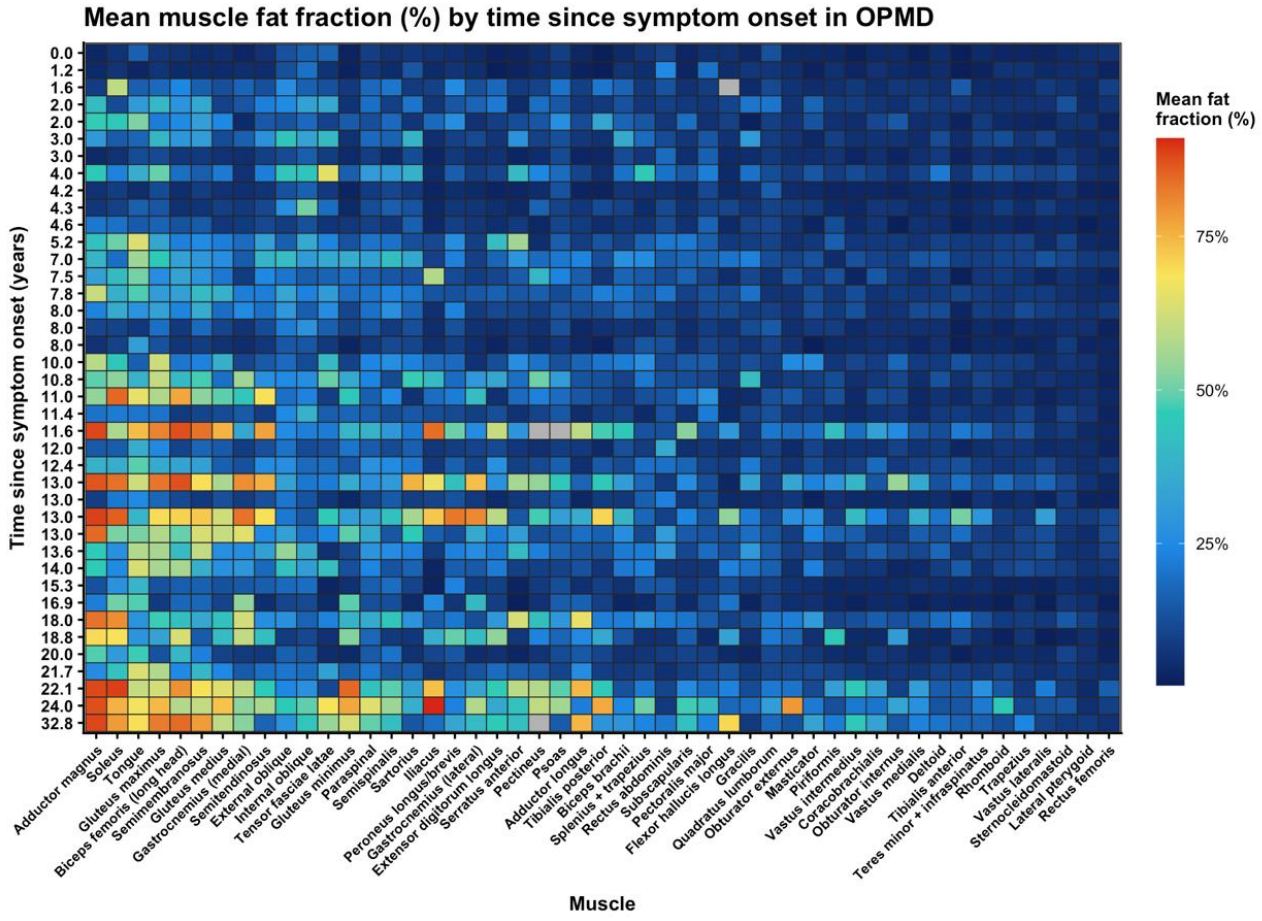

Figure 2: Heatmap of fat replacement pattern versus time since symptom onset and qMRI measure in OPMD participants. Each row represents a patient arranged in ascending order, by time since symptom onset to qMRI. Each column represents a muscle, ordered by the mean FF across all participants; left and right sides are averaged within each participant. This heatmap highlights the muscle-specific pattern of fat replacement across ages in OPMD. The greatest increase in FF was seen in adductor magnus, biceps femoris (long head), semimembranosus, semitendinosus, and adductor longus, whereas rectus femoris, vastus lateralis, and vastus intermedius showed smaller overall FF. This trend indicates toward greater fat fraction with increasing disease duration and age.

FF differences between OPMD and controls

Figure 3 exhibits the greatest increases in FF were seen in the adductor magnus, the biceps femoris (long head), the semimembranosus, the semitendinosus, and the adductor longus, whereas lower-fat muscles such as rectus femoris, vastus lateralis, and vastus intermedius showed smaller or non-significant differences. This pattern is consistent with selective thigh muscle involvement in OPMD, with greater separation from controls in the more fat-infiltrated muscles.

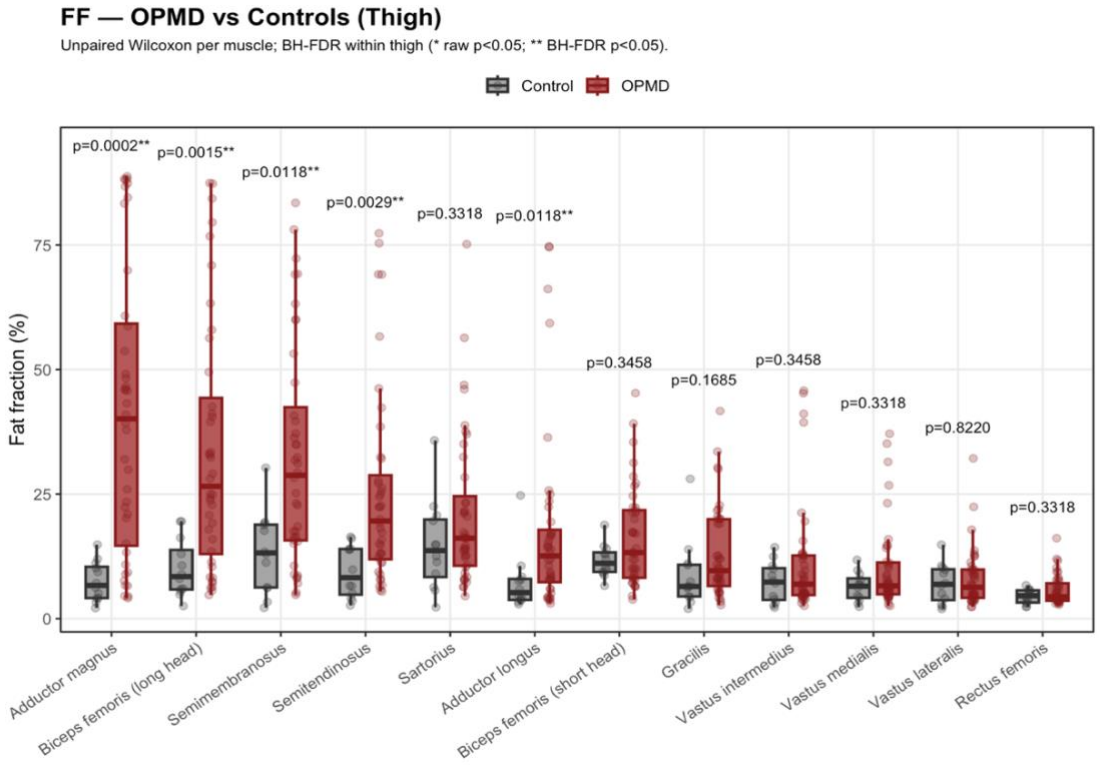

Figure 3: Differences between OPMD participants and controls in high FF muscles: Boxplots show the distribution of FF values in thigh muscles for patients with OPMD and controls, with muscles ordered from highest to lowest mean FF in the OPMD group. Each point represents an individual muscle measurement, with left and right sides averaged for each muscle. Comparisons were performed using unpaired Wilcoxon tests for each muscle, with Benjamini–Hochberg false discovery rate (BH-FDR) correction applied across thigh muscles. P values displayed above each muscle correspond to BH-FDR-adjusted values; ** indicates BH-FDR p < 0.05.

Sex-based and age-based variation in sentinel-muscle fat fraction

Among OPMD participants, males tended to show higher mean FF than females across several sentinel muscles, although the magnitude of this difference varied by muscle and was statistically significant only for biceps femoris (long head) in this analysis, and males were also found to be slightly older than female population in the OPMD group (**Figure 1).** The remaining sentinel muscles showed same general trend, suggesting that sex-related differences may be present but are not significant across all high-fat muscles. When the five sentinel muscles were combined into a participant-level summary measure, sentinel-muscle FF showed a strong positive association with age in both female and male OPMD participants, whereas no significant age relationship was seen in controls (**Figure 4B**). Together, these findings suggest that in OPMD, fat replacement in the most affected thigh muscles increases with age in both sexes, while further analysis is needed to better define sex differences at the individual muscle level.

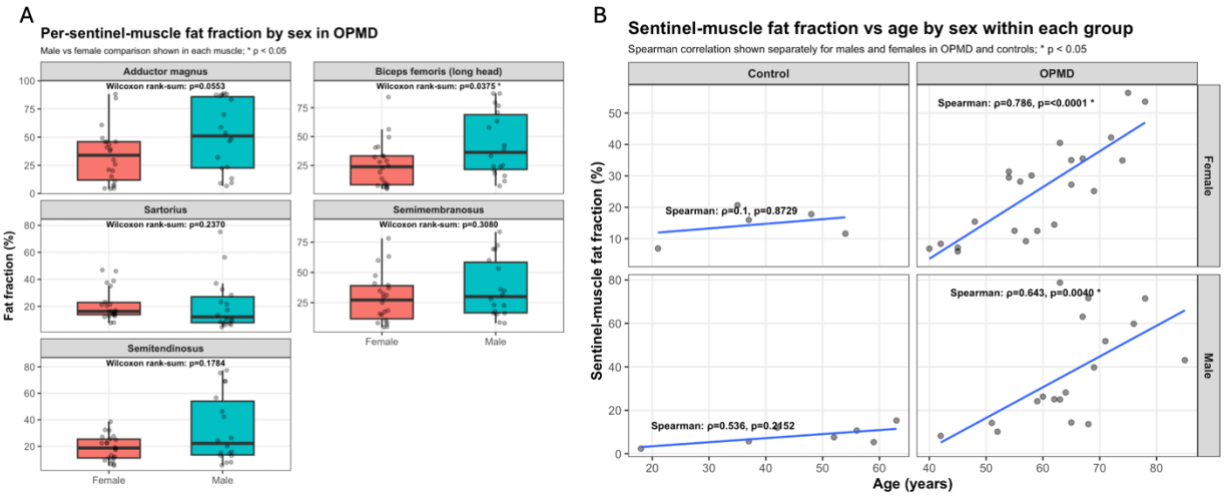

Figure 4: Sex-based differences and age associations in sentinel-muscle FF. (A) Boxplots show FF in the five sentinel thigh muscles in male and female OPMD participants, with individual data points overlaid. The sentinel muscles were defined as the five thigh muscles with the highest mean FF in OPMD: adductor magnus, biceps femoris (long head), sartorius, semimembranosus, and semitendinosus. P values above each panel indicate the male-versus-female comparison within OPMD for each muscle. (B) Scatterplots show the relationship between participant-level sentinel-muscle FF and age, stratified by sex and group. Sentinel-muscle FF was calculated as the mean FF across the five sentinel muscles. Spearman correlation coefficients and p values are shown separately for female and male controls and for female and male OPMD participants.

Correlation between high FF muscles and ADC in thigh compartment in the OPMD cohort

Highly fat replaced muscles of the thigh show a strong, significant, negative correlation between FF and ADC ($p < 0.0001$) as indicated in **Figure 5**. Muscles such as the adductor magnus ($\rho = -0.90$), biceps femoris ($\rho = -0.87$), semimembranosus ($\rho = -0.93$), and semitendinosus ($\rho = -0.84$) demonstrated stronger negative correlations between FF and ADC, suggesting that increasing fat infiltration is associated with reduced water diffusivity, likely due to alterations in the tissue microstructure accompanying fatty replacement. Muscles that are less fat affected in the thigh compartment such as the rectus femoris have very weak non-significant association between FF-ADC. **Figure 5A** scatter plot also indicates that certain muscles might have ADC values independent of the disease activity, as indicated by the low FF muscles on the left side of the x axis where certain muscles group such as the in the quadriceps (vastus) anterior compartment of the thigh have higher mean ADC values and the rectus femoris is having lower mean ADC values, independent of disease activity. To assess a whole-body correlation a forest plot is exhibited in the Appendix section as **Supplemental Figure 2**.

A

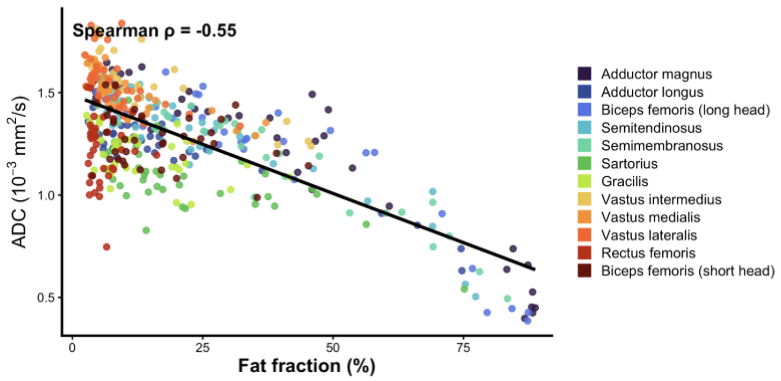

B

Thigh — FF vs ADC (OPMD)

Muscle	Mean FF (%) ± SD	Spearman ρ	Bonferroni p
Adductor magnus	41.2 ± 28.9	-0.90	<0.0001
Biceps femoris (long head)	33.8 ± 25.2	-0.87	<0.0001
Semimembranosus	32.5 ± 22.3	-0.93	<0.0001
Semitendinosus	25.4 ± 19.7	-0.84	<0.0001
Sartorius	21.1 ± 15.4	-0.65	0.0001
Adductor longus	18.0 ± 18.7	-0.70	<0.0001
Biceps femoris (short head)	16.4 ± 10.0	-0.24	1.0000
Gracilis	13.2 ± 9.2	-0.46	0.0518
Vastus intermedius	11.5 ± 11.5	-0.67	<0.0001
Vastus medialis	10.2 ± 8.7	-0.75	<0.0001
Vastus lateralis	8.1 ± 5.9	-0.66	0.0001
Rectus femoris	5.8 ± 3.0	-0.02	1.0000

Figure 5: Relationship between FF and ADC across thigh muscles in OPMD participants demonstrating stronger negative correlation in high FF muscles. Figure 5A shows the association between FF and ADC across thigh muscles in patients with OPMD. Each point represents a muscle-level measurement. Overall, FF and ADC showed a moderate negative correlation (Spearman ρ = −0.55), indicating lower ADC values with increasing fat replacement. The table in Figure 5B represents the individual muscle summary of mean FF. Spearman correlation coefficients, and Bonferroni-corrected p values for the association are shown between FF and ADC in individual thigh muscles. Figure 5A indicates that as the FF increases the diffusivity decreases, and the negative correlation strength is stronger in higher FF muscles as shown in the Table 5B.

ADC differences between OPMD and controls

Figure 6 highlights muscles with higher fat replacement e.g., the adductor magnus, the biceps femoris long head and the semitendinosus showed significant lower ADC values in the OPMD group compared with controls on unpaired Wilcoxon testing. Overall, this trend suggest that the reduction in diffusivity is most evident in the more fat-replaced muscles in OPMD.

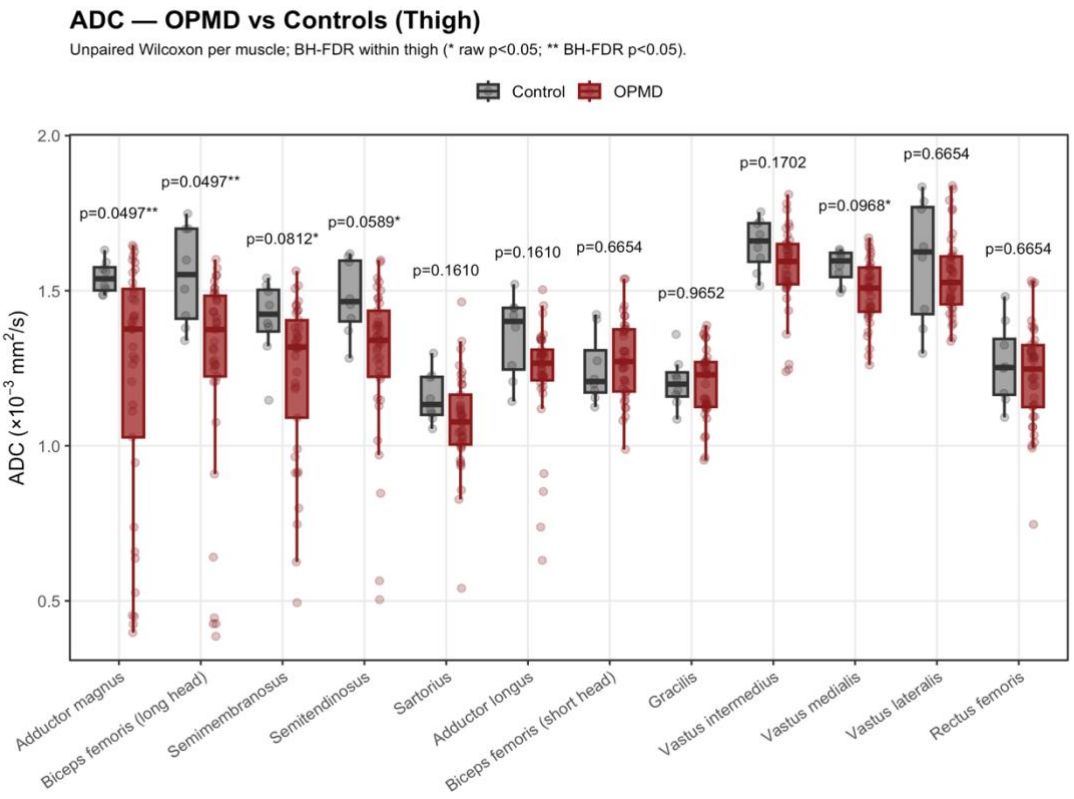

Figure 6: Apparent diffusion coefficient differences in muscles of the thigh with high FF between OPMD participants and controls. Each point represents an individual muscle measurement, with left and right sides averaged for each muscle. Comparisons were performed using unpaired Wilcoxon tests for each muscle, with Benjamini–Hochberg false discovery rate (BH-FDR) correction applied across thigh muscles. P values displayed above each muscle correspond to BH-FDR-adjusted values; ** indicates BH-FDR $p < 0.05$. Muscles such as the adductor magnus and biceps femoris showed lower ADC values in OPMD than in controls, while several other thigh muscles showed a nonsignificant difference.

Correlation between FF and IVIM D in the thigh muscles (OPMD cohort)

High FF muscles of thigh show strong negative correlation with IVIM D. **Figure 7B** shows several muscles have a strong negative correlation between FF and IVIM D, the adductor magnus (ρ =-0.89), the biceps femoris long head (ρ =-0.89), the semimembranosus (ρ =-0.88). Like ADC, correlation with low FF muscles is very weak and not significant. These findings suggest that IVIM D decreases as fat replacement increases, particularly in muscles with greater disease involvement.

A

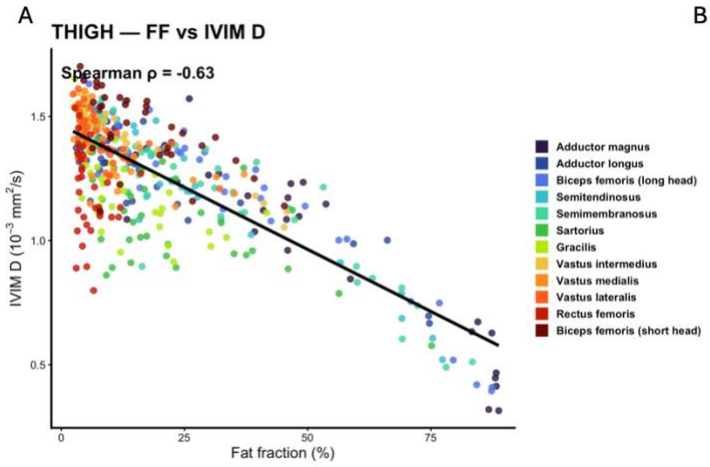

B

Thigh — FF vs IVIM D (OPMD)

Muscle	Mean FF (%) ± SD	Spearman ρ	Bonferroni p
Adductor magnus	41.2 ± 28.9	-0.89	<0.0001
Biceps femoris (long head)	33.8 ± 25.2	-0.89	<0.0001
Semimembranosus	32.5 ± 22.3	-0.88	<0.0001
Semitendinosus	25.4 ± 19.7	-0.87	<0.0001
Sartorius	21.1 ± 15.4	-0.47	0.0380
Adductor longus	18.0 ± 18.7	-0.64	0.0002
Biceps femoris (short head)	16.4 ± 10.0	-0.62	0.0017
Gracilis	13.2 ± 9.2	-0.74	<0.0001
Vastus intermedius	11.5 ± 11.5	-0.83	<0.0001
Vastus medialis	10.2 ± 8.7	-0.69	<0.0001
Vastus lateralis	8.1 ± 5.9	-0.66	0.0001
Rectus femoris	5.8 ± 3.0	-0.24	1.0000

Figure 7: Correlation between FF and IVIM D: Figure 7A scatter plot showing the relationship between FF and IVIM D across thigh muscles in patients with OPMD. Each point represents a muscle-level measurement. Overall, FF and IVIM D showed a moderate negative correlation (ρ = −0.63), indicating lower diffusivity with increasing fat replacement. The table in Figure 7B represents: Individual muscle mean FF, Spearman correlation coefficients, and Bonferroni-corrected p values for the association between FF and IVIM D in individual thigh muscles showing a strong negative correlation between FF-IVIM D in highly fat replaced muscles.

IVIM D differences between OPMD and controls

Figure 8 exhibits IVIM D in the OPMD group compared with controls on unpaired Wilcoxon testing across thigh muscles, IVIM D differed between OPMD and controls. Several muscles, including the adductor magnus, the biceps femoris (long head), the semimembranosus, the semitendinosus, and the adductor longus, showed lower IVIM D values in OPMD than in controls, whereas other thigh muscles showed smaller or non-significant differences. Indicating high FF muscles in OPMD have significant lower diffusivity as compared to controls.

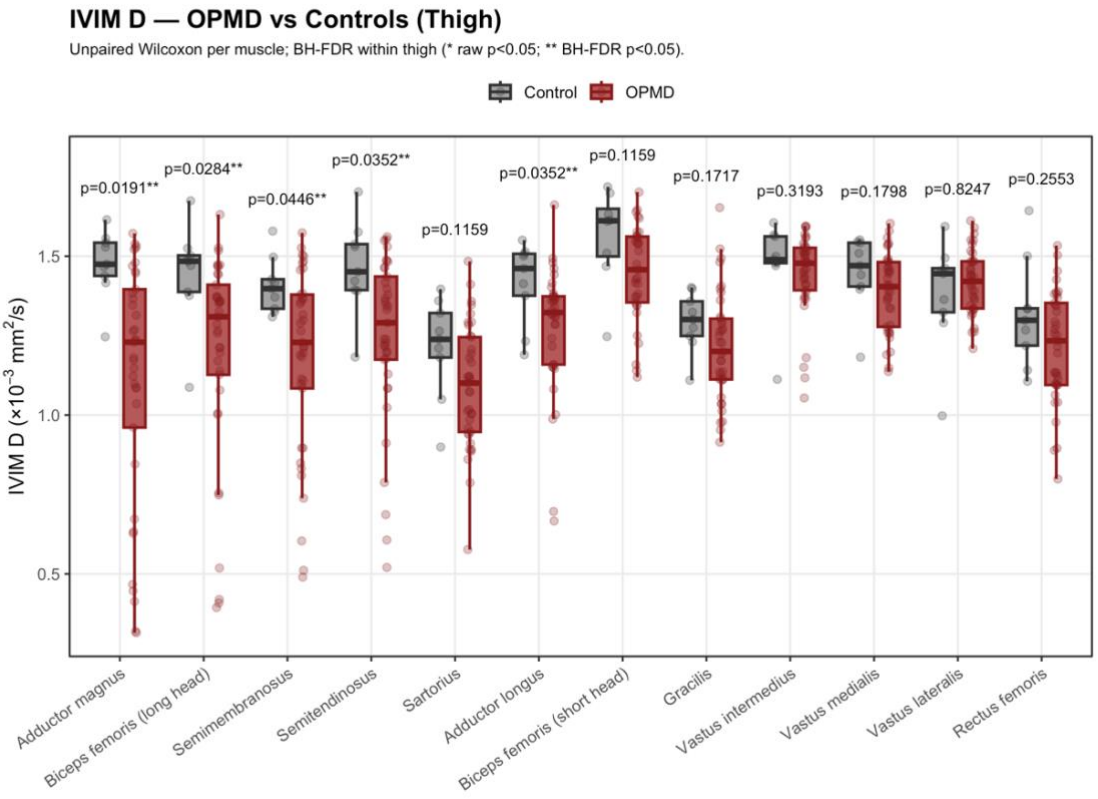

Figure 8: IVIM (D) differences between OPMD group and controls when assessing high FF muscles of thigh region. Each point represents an individual muscle measurement, with left and right sides averaged for each muscle. Comparisons were performed using unpaired Wilcoxon tests for each muscle, with (BH-FDR) correction applied across thigh muscles. P values displayed above each muscle correspond to BH-FDR-adjusted values; ** indicates BH-FDR $p < 0.05$. The figure shows that muscles with greater fat replacement, including adductor magnus, biceps femoris (long head), semimembranosus, semitendinosus, and adductor longus, tended to have lower IVIM D values in OPMD than in controls, whereas less fat-infiltrated muscles showed smaller or non-significant differences. This suggests that reduced IVIM D is more closely seen in muscles with greater disease FF involvement.

Correlation between IVIM F and FF

Overall, in **Figure 9A** FF showed only a weak positive association with IVIM F across thigh muscles ($\rho = 0.28$). When examined by disease-duration period, significant positive correlations after BH-FDR correction were seen only in selected muscles like the adductor magnus and the biceps femoris in early disease period as exhibited

in **Figure 9B**. As the IVIM F is the perfusion fraction possibly related to blood supply to the muscle, this could indicate an increase in microvasculature due to increase in oxidative and metabolic demand in early disease stages where there is increased fat replacement. Figure 9B forest plot demonstrates a strong positive association between FF and IVIM F in early disease duration (0-5 years) in muscles known to have high FF, such as the adductor magnus and the biceps femoris long head, whereas the correlation strength becomes negative in later disease duration (10-15, 15+ years), which could highlight decreased disease activity due to either ceiling effect or muscle atrophy.

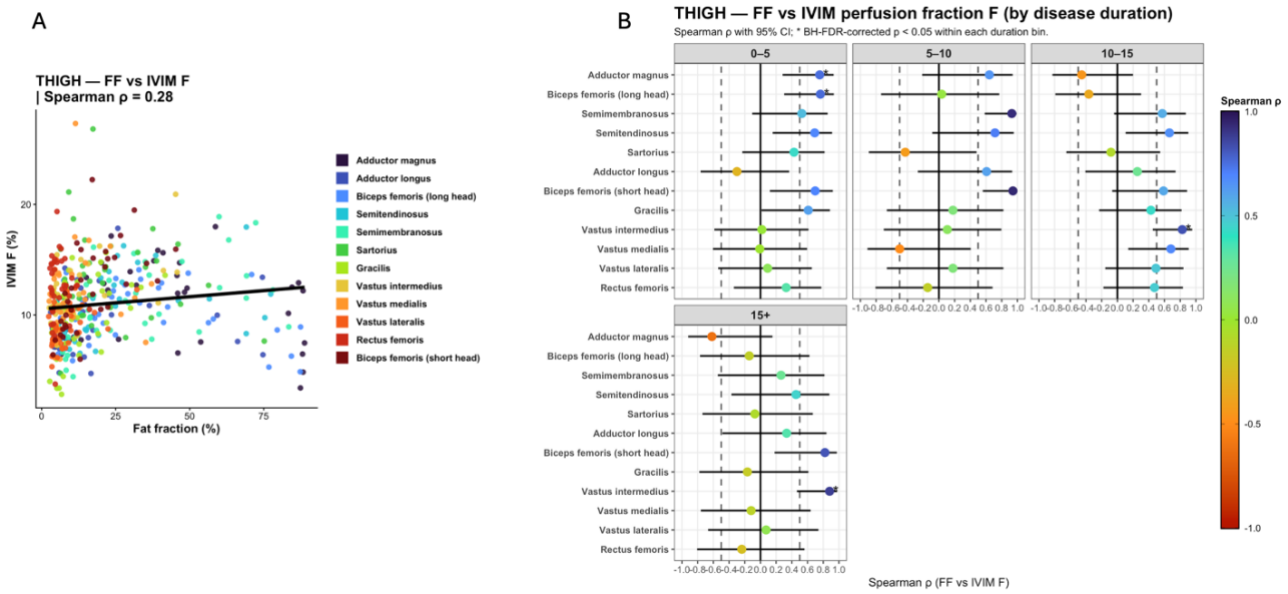

Figure 9: Relationship between FF and IVIM F across thigh muscles in OPMD, overall and by disease duration. Each point represents a muscle-level measurement, coloured by muscle. Overall, FF showed a weak positive correlation with IVIM F (Spearman ρ = 0.28). Figure 9B represents: Spearman correlation coefficients with 95% confidence intervals for the association between FF and IVIM F, stratified by disease-duration period (0–5, 5–10, 10–15, and 15+ years) the dotted line represents moderate correlation strength. Correlations were corrected within each duration bin using the FDR-BH. The results show that the relationship between FF and IVIM F varies by muscle and disease stage, and that association strength between FF and IVIM F might indicate stages of disease activity.

Comparison of IVIM F between OPMD participants and control group

IVIM F values were compared between OPMD participants and controls across thigh muscles using unpaired Wilcoxon tests with BH-FDR correction as exhibited in **Figure 10**. Overall, most thigh muscles showed no significant difference between groups after correction, indicating no differences in IVIM F values between OPMD and controls. A significant increase was seen in the adductor magnus at the raw p-value level, but this did not remain significant after BH-FDR correction. These findings suggest that, unlike FF and diffusivity measures, IVIM F does not show a consistent separation between OPMD and control thigh muscles in this cohort at a cross-sectional level.

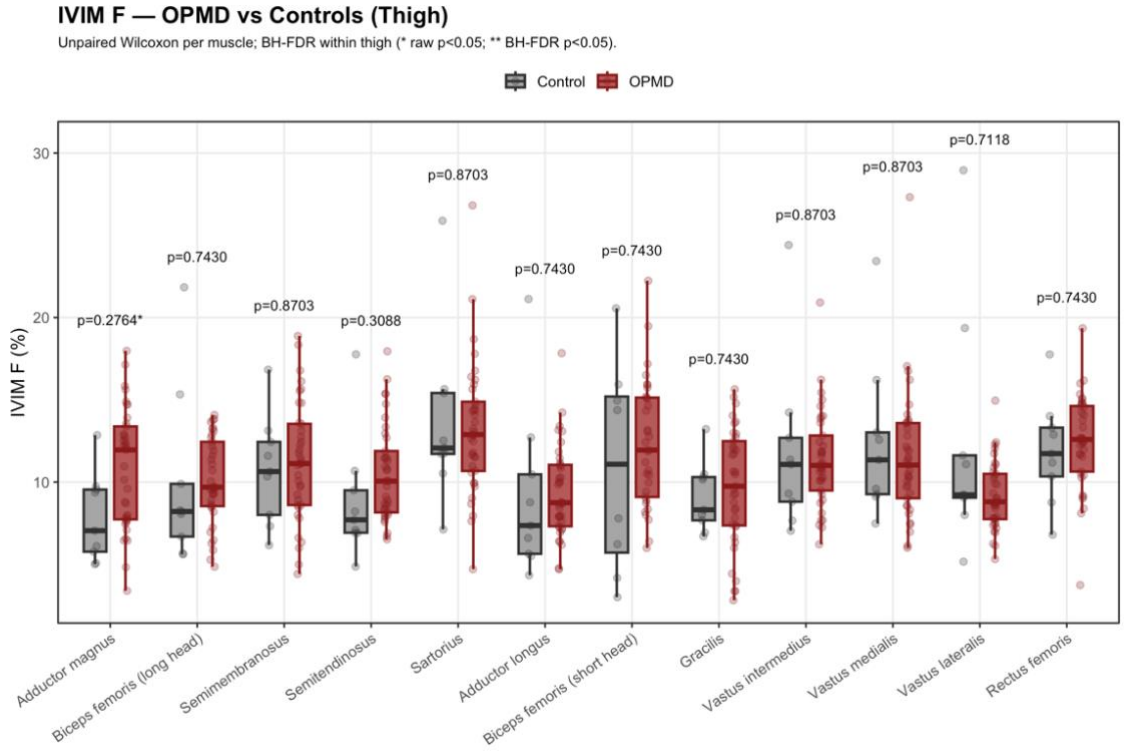

Figure 10: IVIM F values for OPMD and control group for high FF muscles, no significant differences between OPMD participants and controls when assessing with IVIM F. Each point represents an individual muscle measurement, with left and right sides averaged for each muscle. Comparisons were performed using unpaired Wilcoxon tests for each muscle, with (FDR-BH) correction applied across thigh muscles. P values displayed above each muscle correspond to BH-FDR-adjusted values; ** indicates BH-FDR $p < 0.05$. Overall, IVIM F values

showed substantial overlap between OPMD and control muscles, with no consistent significant differences after correction.

Relationship between thigh muscle FF and IVIM D* in OPMD

Across thigh muscles in OPMD, IVIM D* showed a weak overall negative trend with FF, with the pooled analysis demonstrating a Spearman correlation of ρ = -0.30 **Figure 11**. At the individual muscle level, the direction of association was also generally negative, although the strength was moderate to weak, not significant and variable across muscles. The strongest inverse relationships were observed in semimembranosus and adductor longus, whereas some muscles such as sartorius showed little apparent trend. After Bonferroni correction, none of the muscle-specific associations remained statistically significant. Overall, these findings suggest that pseudo-diffusion tends to decrease with increasing fat replacement in OPMD thigh muscles, but the relationship is relatively weak and less consistent than that observed for diffusion measures.

A

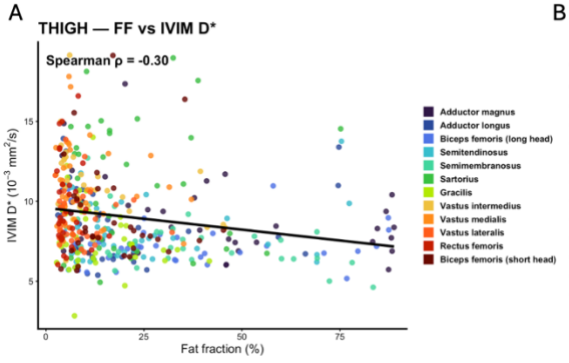

B

Thigh — FF vs IVIM D* (OPMD)

Muscle	Mean FF (%) ± SD	Spearman ρ	Bonferroni p
Adductor magnus	41.2 ± 28.9	-0.33	0.5896
Biceps femoris (long head)	33.8 ± 25.2	-0.12	1.0000
Semimembranosus	32.5 ± 22.3	-0.43	0.0984
Semitendinosus	25.4 ± 19.7	-0.00	1.0000
Sartorius	21.1 ± 15.4	0.02	1.0000
Adductor longus	18.0 ± 18.7	-0.38	0.2350
Biceps femoris (short head)	16.4 ± 10.0	-0.07	1.0000
Gracilis	13.2 ± 9.2	-0.16	1.0000
Vastus intermedius	11.5 ± 11.5	-0.38	0.2543
Vastus medialis	10.2 ± 8.7	-0.12	1.0000
Vastus lateralis	8.1 ± 5.9	-0.13	1.0000
Rectus femoris	5.8 ± 3.0	-0.17	1.0000

Figure 11: Association between thigh muscle fat fraction and IVIM D* in OPMD. The left panel shows the relationship between FF and IVIM D* across 12 thigh muscles in participants with OPMD, using left-right averaged values for each muscle. Each point represents one muscle-level observation and is colour-coded by muscle. The pooled Spearman correlation coefficient is shown on the plot. The right panel summarizes, for each muscle, the mean FF ± SD together with the muscle-specific Spearman correlation coefficient and Bonferroni-adjusted p value for the association between FF and IVIM D*. Muscles are presented in descending order of mean FF.

Comparison of IVIM D* between OPMD participants and control group

IVIM D* values in thigh muscles showed no significant differences between patients with OPMD and controls after correction for multiple comparisons, as shown in **Figure 12**. Although semimembranosus showed a nominal raw p-value difference, the overall pattern between groups across most thigh muscles, exhibits that pseudo-diffusion does not clearly distinguish OPMD from controls in this cohort when analysing at a cross-sectional level. Inclusion of a larger number of age-matched controls and extension into longitudinal analysis may help clarify whether IVIM D* changes emerge with disease progression or vary across specific muscles over time.

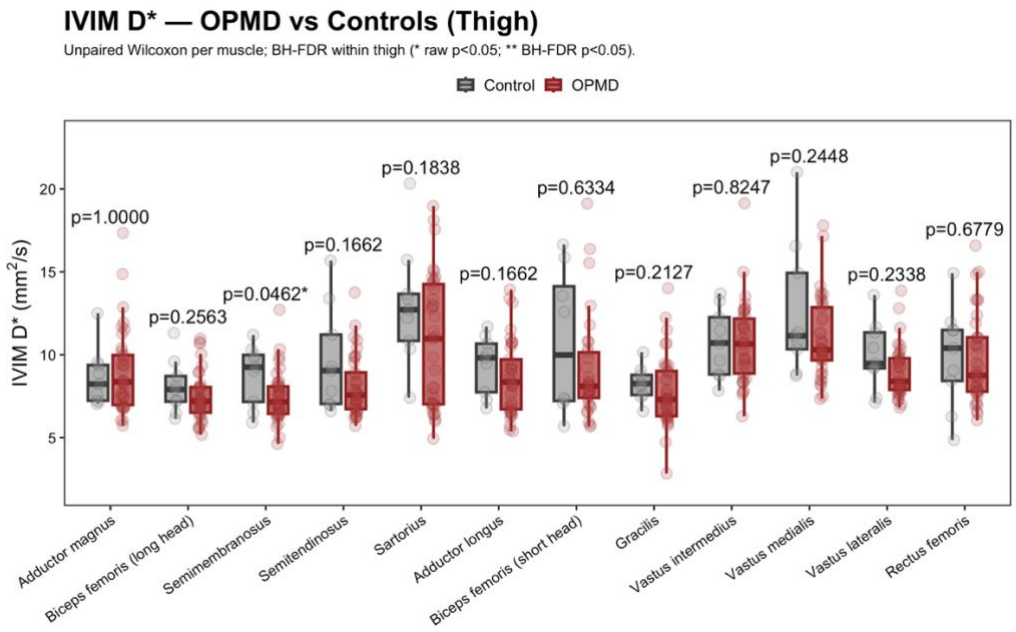

Figure 12: Comparison of thigh IVIM D* between OPMD and controls. Boxplots show left-right averaged IVIM D* values for 12 thigh muscles in participants with OPMD and controls. Individual subject values are overlaid as jittered points. For each muscle, groups were compared using unpaired Wilcoxon rank-sum tests, and p values are shown above the corresponding muscle. FDR-BH was applied within the thigh muscle set; ** indicates BH-FDR-adjusted $p < 0.05$. Overall, most muscles showed no differences between the two groups.

Correlation between FF and T2 relaxation time

T2 relaxation time showed only a weak overall positive trend with FF (Spearman $\rho = 0.18$) (Figure 13A). Analyses also showed generally weak and inconsistent correlations, with no robust significant associations remaining after Bonferroni correction, despite some nominal positive trends in selected muscles. A similar trend was seen with

perfusion fraction in **Figure 9B**; the strength and direction of these relationships may vary across stages of disease activity. A positive correlation was observed in certain muscles like the sartorius, adductor longus and vastus medialis and may indicate disease activity (i.e. fat infiltration) in Table 13B, however with weak non-significant trend, this would need to be assessed more in a longitudinal setting to assess if water sensitive markers like T2 relaxation time can track disease progression and severity like FF.

A

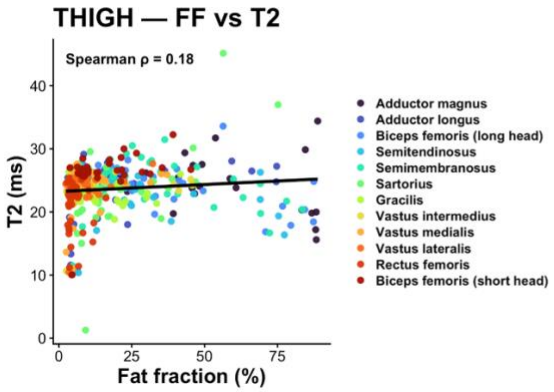

B

Thigh — FF vs T2 (OPMD)

Muscle	Mean FF (%) ± SD	Spearman ρ	Bonferroni p
Adductor magnus	41.2 ± 28.9	-0.13	1.0000
Biceps femoris (long head)	33.8 ± 25.2	-0.35	0.4973
Semimembranosus	32.5 ± 22.3	-0.26	1.0000
Semitendinosus	25.4 ± 19.7	-0.28	1.0000
Sartorius	21.1 ± 15.4	0.59	0.0026
Adductor longus	18.0 ± 18.7	0.33	0.6045
Biceps femoris (short head)	16.4 ± 10.0	0.28	1.0000
Gracilis	13.2 ± 9.2	-0.15	1.0000
Vastus intermedius	11.5 ± 11.5	0.16	1.0000
Vastus medialis	10.2 ± 8.7	0.39	0.2506
Vastus lateralis	8.1 ± 5.9	0.28	1.0000
Rectus femoris	5.8 ± 3.0	0.10	1.0000

Figure 13: Correlation between FF and T2 relaxation time: Figure 13A showing the association between FF and T2 relaxation time across thigh muscles in patients with OPMD. Each point represents a muscle-level measurement. Overall, FF and T2 showed a weak positive trend (ρ = 0.18). Figure 13B: Individual muscle summary of mean FF, Spearman correlation coefficients, and Bonferroni-corrected p values for the association between FF and T2 in individual thigh muscles. Correlations were generally weak and heterogeneous across muscles, with no robust associations remaining after Bonferroni correction, although nominal positive trends were seen in selected muscles such as the sartorius, the adductor longus, the vastus medialis, and the vastus lateralis. These findings suggest that the relationship between fat replacement and T2 relaxation time is variable across thigh muscles in OPMD at a cross-sectional level and more needs to be assessed with a longitudinal timepoint.

Comparison of the muscle T2 relaxation times between OPMD participants and controls

T2 relaxation time values in thigh muscles showed no significant differences between patients with OPMD and controls as exhibited in **Figure 14**. Although the semitendinosus showed a nominal raw p-value difference, the overall pattern suggests that T2 relaxation time does not clearly distinguish OPMD from controls across most thigh muscles in this cohort. Addition of more aged, matched controls and extending into a longitudinal study could give more insight into the T2 relaxation time pattern in the OPMD group.

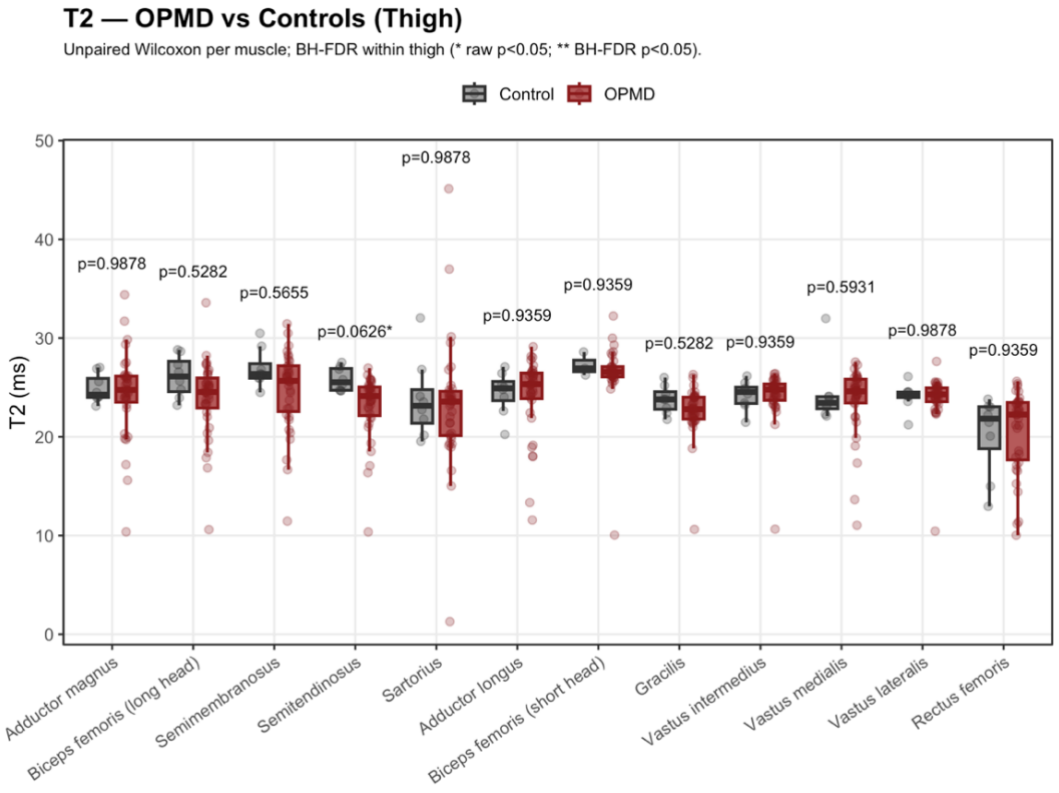

Figure 14: Difference between OPMD participants and controls on T2 relaxation time. Each point represents an individual muscle measurement, with left and right sides averaged for each muscle. Comparisons were performed using unpaired Wilcoxon tests for each muscle, with (FDR-BH) correction applied across thigh muscles. P values displayed above each muscle correspond to BH-FDR-adjusted values; ** indicates BH-FDR $p < 0.05$. Overall, T2 values showed no significant differences between OPMD group and controls, although semitendinosus showed a nominal difference at the raw p-value level. These findings suggest that T2 relaxation time does not clearly distinguish OPMD from controls across most thigh muscles in this cohort.

Cross-sectional pattern of fat replacement across disease-duration period

Figure 15 and 16 exhibits mean FF increased with disease duration, and the spread of FF values became wider in the later duration groups, showing greater variability between participants as disease duration increased. In this cross-sectional analysis, high FF suggests increased disease severity but does not assess disease progression. Muscles with high FF may already be present and progress faster in the early (5-10 year) disease course and then increase at different rates across patients over time. The grey control band in **Figure 15** represents the control group interquartile range (IQR) and provides reference values y axis represents the FF and x axis represents the disease duration periods. This shows that in OPMD participants, the mean FF increases relative to controls with longer disease duration.

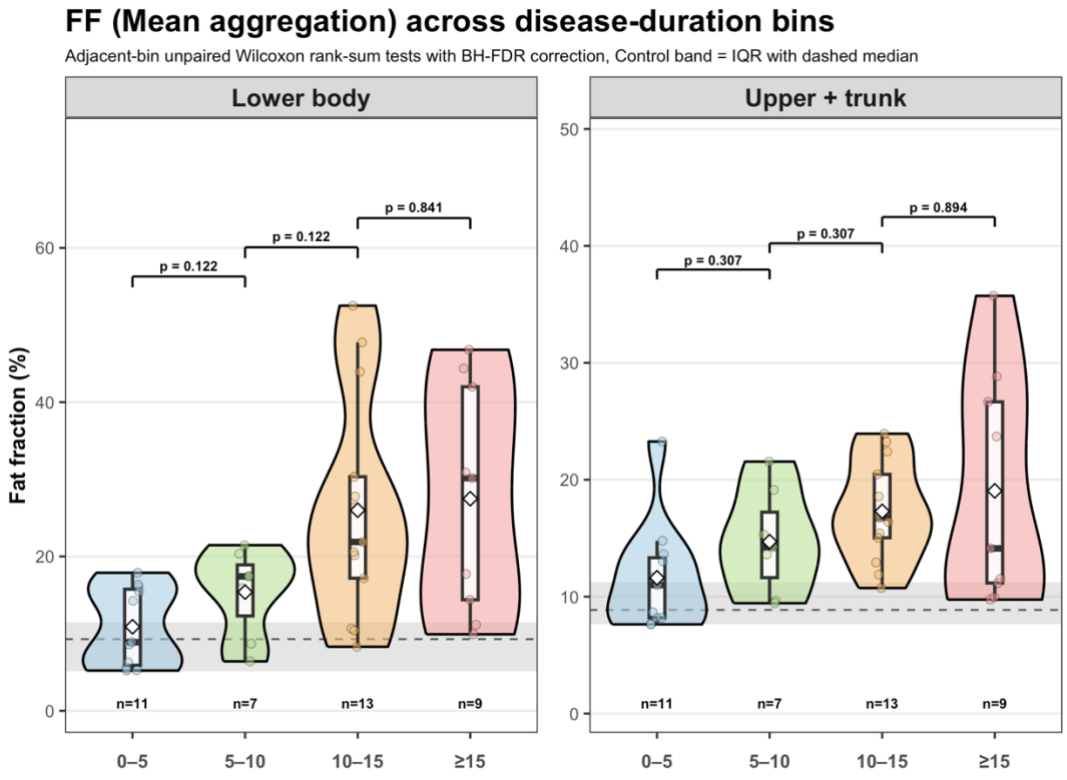

Figure 15: Mean FF across disease-duration bins in lower-body and upper/trunk muscle regions. Violin plots show the distribution of subject-level mean FF values across disease-duration bins (0–5, 5–10, 10–15, and ≥15 years) for the lower body and upper/trunk regions. Within each violin, the boxplot summarizes the interquartile range and median, individual points represent subjects, and the white diamond denotes the group mean. The grey horizontal band represents the control interquartile range (IQR), and the dashed horizontal line within that

band indicates the control median. Adjacent-bin unpaired Wilcoxon rank-sum tests with BH-FDR correction were performed separately within each region, with adjusted p values shown above the brackets and an * indicating statistical significance.

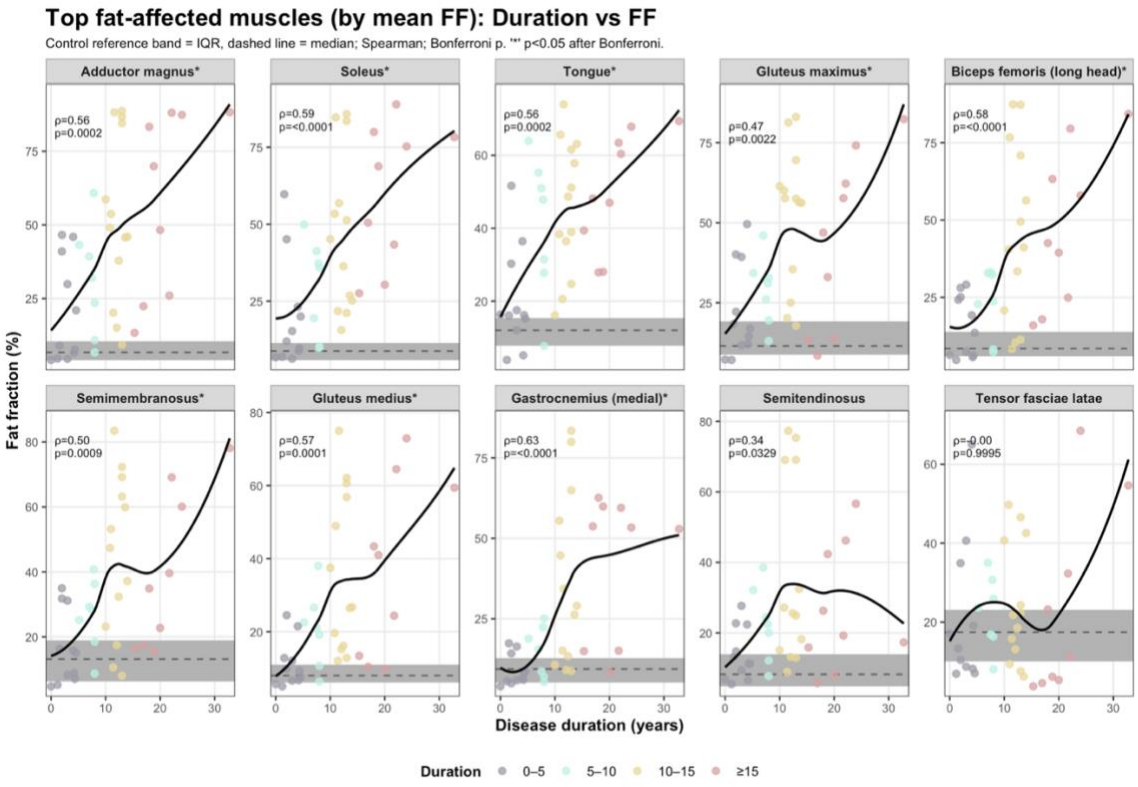

Figure 16: Correlations between FF and disease duration for the 10 most fat-affected muscles. Scatter plots show FF versus disease duration for the 10 muscles with the highest mean FF. Points are colored by disease-duration s (0–5, 5–10, 10–15, ≥15 years). The locally estimated scatterplot smoothing line represents the trend. Each panel reports the Spearman correlation (ρ) between duration and FF with Bonferroni-corrected p-values. FF generally increases with longer disease duration, with several muscles demonstrating significant monotonic correlations after Bonferroni correction.

Cross-sectional pattern of ADC across disease-duration period

Figure 17 and 18 exhibits median ADC values remain close to the control median in the early stage of disease and then show a downward trend with longer disease duration. In contrast to what would be expected if ADC captured an earlier phase of active disease before fat replacement, there is no clear rise in absolute diffusivity values before further increases in FF in the earlier disease duration period. Instead, ADC appears to stay near

the control range at the outset and then gradually decline, which could be consistent with increasing FF. Although this is cross-sectional analysis provides only an indirect view of progression, the overall pattern does not show a clear early elevation in ADC.

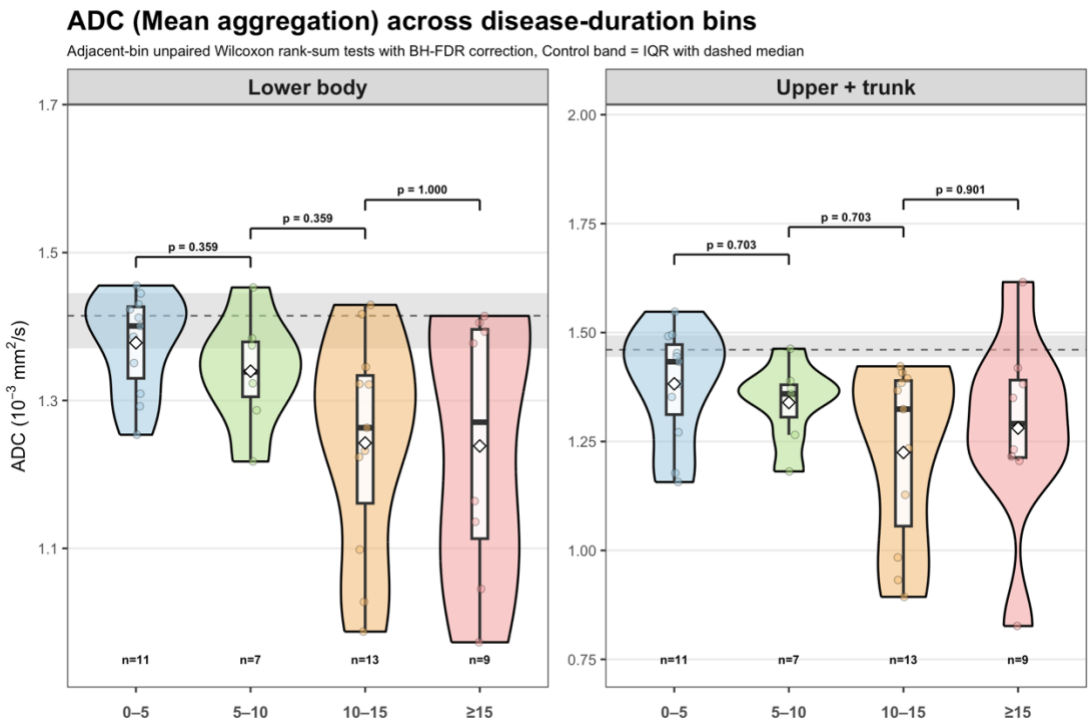

Figure 17: Mean composite ADC values decrease with disease duration. Violin plots show the distribution of subject-level mean ADC values across disease-duration bins (0–5, 5–10, 10–15, and ≥15 years) for the lower body and upper/trunk regions. Within each violin, the boxplot summarizes the interquartile range and median, individual points represent subjects, and the white diamond denotes the group mean. The grey horizontal band represents the control (IQR), and the dashed horizontal line within that band indicates the control median. Adjacent-bin unpaired Wilcoxon rank-sum tests with BH-FDR correction were performed separately within each region, with adjusted p values shown above the brackets. No adjacent-bin comparisons were significant in either region, indicating that mean ADC did not show a clear stepwise change and could be prone to more muscle specific variabilities across disease-duration period.

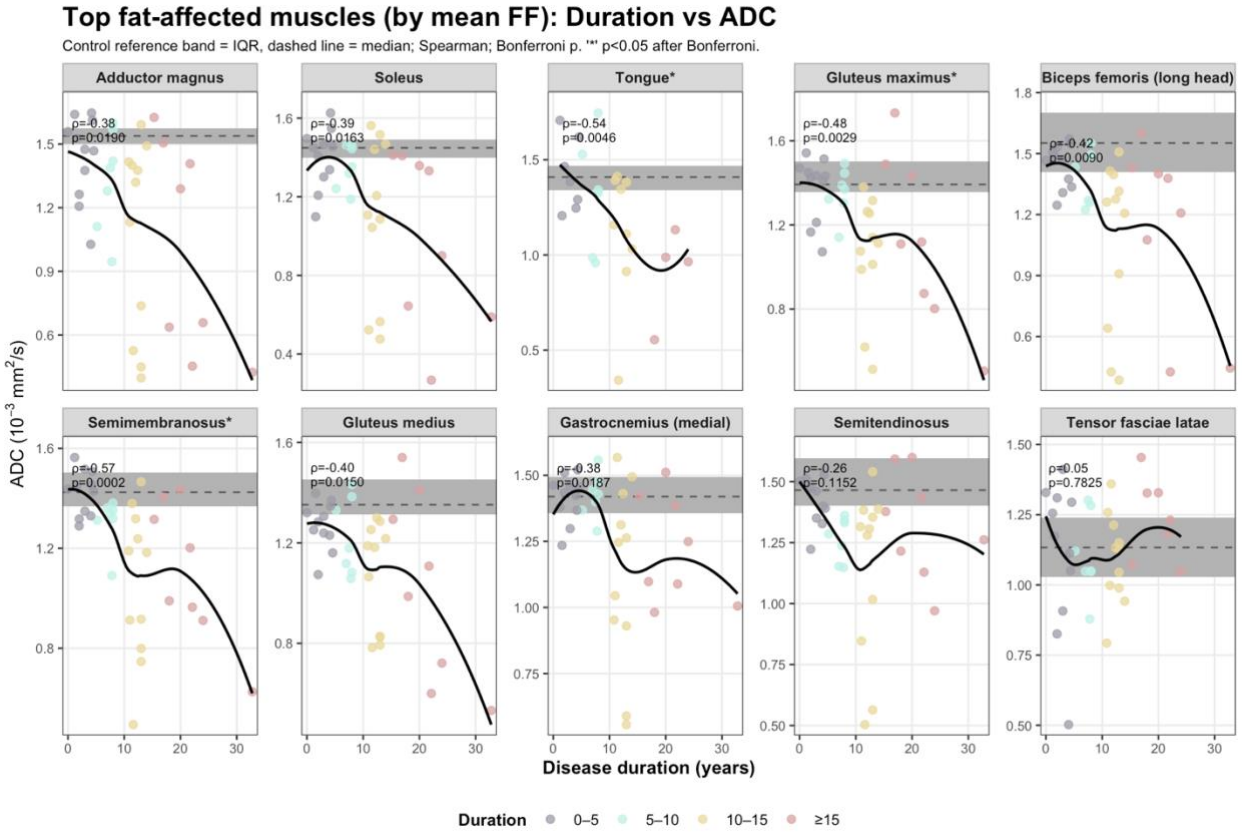

Figure 18: Correlation between diffusivity decreases and disease duration for the 10 most fat affected muscles. Scatter plots show disease duration years versus ADC for the 10 muscles with the highest mean FF. Each point represents one participant and is color-coded by duration strata (0–5, 5–10, 10–15, ≥15 years). The locally estimated scatterplot smoothing line represents the trend. Spearman's ρ and Bonferroni-corrected p-values (across the 10 muscles) are displayed within each panel. ADC generally decreases as disease duration increases, consistent with reduced diffusivity in more advanced disease.

Chapter 4: Discussion

This cross-sectional, muscle qMRI study shows a significant negative correlation between FF and diffusivity measures (ADC and IVIM D) in OPMD. This negative monotonic relationship (meaning as the FF increased, the diffusivity decreased) was more pronounced in muscles with higher degrees of fat replacement including adductor magnus, biceps femoris long head and the soleus suggesting that diffusivity metrics are strongly influenced by the extent of fat replacement in more severely affected muscles. These findings could indicate that as the FF increased the diffusivity or the movement of water molecules decreased due to reduced extracellular space or fat replacement [38,48,49]. Studies assessing diffusivity values between muscular dystrophies (MD) and myositis found MD having lower ADC values, and that there was a significant negative correlation between FF and Diffusivity measures in fat affected muscles in slowly progressive MD [49,50,52]. qMRI has been used to assess if earlier signs of disease activity in calpainopathy identified a good correlation between FF and diffusion with clinical assessments [51]. A study which used dual function MRI phantom to evaluate relationship between FF-ADC found that ADC measurements are influenced by both fat content and tissue density, and their effects on ADC are additive and linearly related [53]. However, to the best of our knowledge, no previous studies have assessed correlation between ADC, IVIM D and FF in OPMD.

Perfusion fraction (IVIM F) also showed significant correlation in muscles affected earlier in the disease course in OPMD. In the early disease-duration bin (0–5 years), associations were stronger in more fat-replaced muscles (the adductor magnus, the semimembranosus, and the semitendinosus). In adductor magnus, the FF–IVIM F association appeared to weaken with longer disease duration and became negative without being significant. A possible mechanistic explanation includes that early vascular recruitment during initial disease activity may occur with increasing fat replacement [37], i.e. metabolic/oxidative demand may change as fat infiltration progresses [37]. However, interpretation is limited due to cross-sectional design, and longitudinal data with adequate sample size are required to further assess this correlation. IVIM has been applied extensively in abdominal imaging [54] and neuroimaging/tumor characterization [55]. Prior work using IVIM to distinguish muscular dystrophy from autoimmune myositis reported lower diffusivity and higher perfusion fraction in muscular dystrophy compared with autoimmune myositis [56,61]. Higher perfusion fraction in muscles with pathological spontaneous needle electromyogram activity was reported, indicating association of increased IVIM F with possible inflammatory

changes in the muscle [70]. However, there are still limited studies and higher numbers of patients are needed to identify a clearer analysis of the association between IVIM f with FF and active inflammatory or fat replacement states.

Pseudo-diffusion (IVIM D*) showed a weak overall negative trend with FF. At the individual muscle level, the pattern was heterogeneous, with muscles showing non-significant associations. Semimembranosus showed the strongest negative trend with FF, while adductor magnus and adductor longus showed a weaker negative trend. Since IVIM D* is interpreted as a perfusion-related diffusion parameter reflecting microvascular blood flow in the capillary network rather than true tissue diffusion, this could mean at a cross-sectional level fat replacement could have less influence on IVIM D* [37,80]. However, interpretation remains limited in a cross-sectional analysis, and longitudinal assessment would be needed to assess the correlation better.

T2 relaxation time showed a weak overall positive trend with FF. At the individual muscle level, the pattern was heterogeneous, with most muscles showing non-significant associations. Sartorius showed a moderate positive trend with FF, while muscles of the anterior thigh compartment showed a weak positive association. This suggests that T2 relaxation time may increase with increase in FF in selected muscles, but this relationship was not consistent across the thigh muscles studied. A prior qMRI study in OPMD showed an increase in both overall T2 relaxation time and muscle FF over 13 months in patients, with no increase in controls [41]. This suggests that longitudinal assessment of individual muscles may provide further insight into the relationship between T2 relaxation time and FF in OPMD.

Currently, quantitative diffusion imaging has not been applied to assess OPMD, whereas as studies performed to assess differences between MD and inflammatory myositis have reported increased diffusivity values in inflammatory myositis compared to MD [60,61]. One longitudinal study assessing OPMD showed that the rectus femoris shows relatively low-fat infiltration on MRI despite greater fibrosis on ultrasound [40,59]. Similarly in this study, the rectus femoris demonstrated low FF, consistent with other studies [39–42], together with low diffusivity which could be explained by increased fibrosis restricting water motion and thereby lowering diffusivity even in the absence of marked fat replacement. The muscles that were assessed to have high FF in our study are also the same muscles to have high FF in other OPMD studies, indicating that OPMD might have a distinct pattern of

fat replacement (where the tongue, hip flexors, hamstring, adductor compartment in the thigh and soleus are all major fat replaced muscles amongst other muscles of the body). This could support developing an OPMD specific imaging protocol and diversifying the imaging modalities which could prove to be cost effective for biomarker discovery. One unique aspect of this comprehensive whole-body qMRI assessment is that it highlights high FF in muscles such as the serratus anterior, rectus abdominis, and the internal rotators of the pelvis (iliacus and obturators), which are muscles that are difficult to assess on clinical exam.

When patients were segregated into exploratory disease-duration periods ("bins"), diffusivity values showed a decreasing trend with increasing disease duration, although most muscles did not reach statistical significance. This pattern could indicate that OPMD behaves predominantly as a "fat replacement–driven" MD, consistent with minimal inflammatory changes seen on muscle biopsy [9,57]. Further, increasing fat replacement in muscle progressively reduces the movement of water molecules and hence reduces measurable diffusivity values [48], or alternatively that any early inflammatory-related increase in diffusivity may be obscured by concurrent fat replacement [69,71]. Because diffusivity is inherent to muscle, any ADC reduction may largely reflect increasing fat replacement [52,53]. ADC is also influenced by tissue microstructure/tortuosity (e.g., fibers and cells) [58], the b-values used for its calculation, and muscle characteristics such as fiber type and size [66]. Currently, the effect of all the said factors in the current analysis are unknown and additional analysis with other advanced qMRI measures such as Diffusion Tensor Imaging would be needed in larger longitudinal studies. Furthermore, additional controls and longitudinal follow-up in early disease course is needed to determine whether each muscle has a baseline diffusivity values independent of disease activity.

Even though OPMD is a slowly progressive disorder, there could be increased fat replacement even early in the disease course (5–10-year period). qMRI could aid in earlier monitoring severity and progression, as treating patients before substantial fat replacement, which is currently felt to be an irreversible process [62-64]. High fat replaced muscles also appear to be earlier affected; however, more needs to be analysed to determine the extent and rate of fat replacement, as these may vary across individuals [65], reflected by the large spread in highly fat-replaced muscles in later disease duration. Since this is the first study assessing the correlation between FF and other water measures in OPMD, these preliminary findings can support longitudinal studies, and for future

prospective trials other qMRI measures like the perfusion fraction may prove to be a responsive treatment marker along with FF.

Limitations

This study was cross-sectional, limiting inference about within-subject change and true progression patterns. Although patients were grouped by disease duration (0–5, 5–10, 10–15, and >15 years) to visualize potential trends and to keep bin sizes comparable, this stratification is exploratory and cannot replace longitudinal follow-up. With a larger sample, the optimal duration-based grouping would need re-evaluation to improve robustness and interpretability. Ultimately, a larger, prospective, longitudinal natural history study is required to define fat replacement trajectories and the temporal relationships among qMRI biomarkers.

The ADC sequence, based on the echo-planar image acquisition scheme, can be affected by magnetic field inhomogeneity and phase-encoding chemical shift due to unsuppressed lipid signal, so it is less reliable for smaller muscles next to air interface like the tongue and for more peripheral shoulder muscles which is a limitation in terms of segmentation and analysis. Imaging artifacts resulted in missing muscle measurements in some patients, limiting the current analysis; consequently, upper body correlations which are more sensitive to MRI artifacts from breathing warrant further investigation using optimized imaging protocols. Supplemental table 4 highlight the values of missing muscles group in the upper body.

One of the major limitations is the lack of age matched healthy controls for varied qMRI sequences. ADC values may also vary with age, so a higher number of age-matched controls are needed to interpret muscle ADC values and give more robustness to the analysis, and adding more controls could help in assessing if there is muscle specific value associated with ADC. A study in 116 healthy controls found the mean normal ADC values in the ankle dorsiflexors $1.45 \pm 0.04 \times 10^{-3}$ mm^2/s, and $1.44 \pm 0.06 \times 10^{-3}$ mm^2/s in males and females respectively, similarly for the erector spinae muscles ADC were $1.45 \pm 0.11 \times 10^{-3}$ mm^2/s and $1.52 \pm 0.13 \times 10^{-3}$ mm^2/s in males and females respectively [66]. There was minimal gender- or age-related ADC differences for each muscle, however these values could be interpretated in the context of other muscles and different b values. Control cohort

mean ADC in this study for paraspinal muscle was 1.42 ± 0.06 10^{-3} mm^2/s, ankle dorsiflexors 1.44 ± 0.09 10^{-3} mm^2/s.

For IVIM, we have used segmented nonlinear least squares fitting with b values threshold of 200 s/mm^2 to estimate D, D*, and F. A research study investigating healthy individuals across all muscles, and the values were reported as: D = 1.46 ± 0.30 × 10^{-3} mm^2/s, D* = 29.7 ± 38.1 × 10^{-3} mm^2/s, and f = 11.1 ± 6.7 % [37]. Reported IVIM parameters in back, thigh, and leg muscles showed no significant differences across anatomic locations [37]. In this control group, the composite IVIM D was 1.408 ± 0.101 x 10^{-3} mm^2/s, the pseudo-diffusion coefficient D* was 9.974 ± 1.180 x 10^{-3} mm^2/s, and the perfusion fraction f was 10.74 ± 3.88%.

Slowly progressive MDs such as OPMD can show heterogeneity along the proximodistal muscle gradient, and a single slice covers only a limited section of each muscle [65,67,68]. Prior work segmented the thigh at three levels rather than one slice and still identified the same muscles as fat affected [39]. A broader segmentation protocol potentially supported by automated segmentation could provide more comprehensive characterization of progression and proximodistal gradients [67,68].

Conclusion

In OPMD, higher FF is associated with lower diffusivity measures, most significantly in more fat-replaced muscles. Perfusion fraction showed a weak/moderate positive correlation with FF with certain muscles - and stage-dependent variation, suggesting it may provide complementary physiological information to FF in early disease activity, while pseudo-diffusion and T2 relaxation time showed weak associations in this cross-sectional study. The diffusivity measures (ADC and D) did not rise in early disease activity preceding to fat replacement. As the disease duration increases fat replacement increased, and diffusivity parameters decreased. Future studies would aim to follow patients longitudinally to provide further insight into progression of fat replacement patterns.

Chapter 5: References

1-Brais, B., Bouchard, J. P., Xie, Y. G., Rochefort, D. L., Chrétien, N., Tomé, F. M., Lafrenière, R. G., Rommens, J. M., Uyama, E., Nohira, O., Blumen, S., Korczyn, A. D., Heutink, P., Mathieu, J., Duranceau, A., Codère, F., Fardeau, M., & Rouleau, G. A. (1998). Short GCG expansions in the PABP2 gene cause oculopharyngeal muscular dystrophy. Nature genetics, 18(2), 164–167. https://doi.org/10.1038/ng0298-164

2- Brisson, J. D., Gagnon, C., Brais, B., Côté, I., & Mathieu, J. (2020). A study of impairments in oculopharyngeal muscular dystrophy. Muscle & nerve, 62(2), 201–207. https://doi.org/10.1002/mus.26888

3- Blumen, S. C., Nisipeanu, P., Sadeh, M., Asherov, A., Blumen, N., Wirguin, Y., Khilkevich, O., Carasso, R. L., & Korczyn, A. D. (1997). Epidemiology and inheritance of oculopharyngeal muscular dystrophy in Israel. Neuromuscular disorders: NMD, 7 Suppl 1, S38–S40. https://doi.org/10.1016/s0960-8966(97)00080-1

4- Maksimova, N. R., Nikolaeva, I. A., Korotkov, M. N., Ikeuchi, T., Onodera, O., Nishizava, M., Stepanova, S. K., Kurtanov, K.hA., Sukhomiasova, A. L., Nogovitsyna, A. N., Gurinova, E. E., Stepanov, V. A., & Puzyrev, V. P. (2008). Zhurnal nevrologii i psikhiatrii imeni S.S. Korsakova, 108(6), 52–60.

5- Becher, M. W., Morrison, L., Davis, L. E., Maki, W. C., King, M. K., Bicknell, J. M., Reinert, B. L., Bartolo, C., & Bear, D. G. (2001). Oculopharyngeal muscular dystrophy in Hispanic New Mexicans. *JAMA*, *286*(19), 2437–2440. https://doi.org/10.1001/jama.286.19.2437

6- Alonso-Pérez, J., de León Hernández, J. C., Pérez-Pérez, H., Mendoza-Grimón, M. D., Gutierrez-Martinez, A. J., Hadjigeorgiou, I., Montón-Álvarez, F., González-Quereda, L., Alonso-Jimenez, A., Suárez-Calvet, X., & Díaz-Manera, J. (2022). Clinical and genetic features of a large homogeneous cohort of oculopharyngeal muscular dystrophy patients from the Canary Islands. *European journal of neurology*, *29*(5), 1488–1495. https://doi.org/10.1111/ene.15252

7- Bouchard J. P. (1997). André Barbeau and the oculopharyngeal muscular dystrophy in French Canada and North America. Neuromuscular disorders : NMD, 7 Suppl 1, S5–S11. https://doi.org/10.1016/s0960-8966(97)00074-6

8- Semmler, A., Kress, W., Vielhaber, S., Schröder, R., & Kornblum, C. (2007). Variability of the recessive oculopharyngeal muscular dystrophy phenotype. *Muscle & nerve*, *35*(5), 681–684. https://doi.org/10.1002/mus.20726

9- Brais B. (2009). Oculopharyngeal muscular dystrophy: a polyalanine myopathy. *Current neurology and neuroscience reports*, *9*(1), 76–82. https://doi.org/10.1007/s11910-009-0012-y

10- Trollet, C., Boulinguiez, A., Roth, F., Stojkovic, T., Butler-Browne, G., Evangelista, T., Lacau St Guily, J., & Richard, P. (2001). Oculopharyngeal Muscular Dystrophy. In M. P. Adam (Eds.) et. al., GeneReviews®. University of Washington, Seattle.

11-Dahlqvist, J. R., Widholm, P., Leinhard, O. D., & Vissing, J. (2020). MRI in Neuromuscular Diseases: An Emerging Diagnostic Tool and Biomarker for Prognosis and Efficacy. *Annals of neurology*, *88*(4), 669–681. https://doi.org/10.1002/ana.25804

12- Kroon, R. H. M. J. M., Kalf, J. G., de Swart, B. J. M., van der Sluijs, B. M., Glennon, J. C., Raz, V., van Engelen, B. G., & Horlings, C. G. C. (2021). Longitudinal Assessment of Strength, Functional Capacity, Oropharyngeal Function, and Quality of Life in Oculopharyngeal Muscular Dystrophy. *Neurology*, *97*(15), e1475–e1483. https://doi.org/10.1212/WNL.0000000000012640

13- Beaudart, C., Rolland, Y., Cruz-Jentoft, A. J., Bauer, J. M., Sieber, C., Cooper, C., Al-Daghri, N., Araujo de Carvalho, I., Bautmans, I., Bernabei, R., Bruyère, O., Cesari, M., Cherubini, A., Dawson-Hughes, B., Kanis, J.

A., Kaufman, J. M., Landi, F., Maggi, S., McCloskey, E., Petermans, J., … Fielding, R. A. (2019). Assessment of Muscle Function and Physical Performance in Daily Clinical Practice : A position paper endorsed by the European Society for Clinical and Economic Aspects of Osteoporosis, Osteoarthritis and Musculoskeletal Diseases (ESCEO). Calcified tissue international, 105(1), 1–14. https://doi.org/10.1007/s00223-019-00545-w

14- Guyatt, G. H., Pugsley, S. O., Sullivan, M. J., Thompson, P. J., Berman, L., Jones, N. L., Fallen, E. L., & Taylor, D. W. (1984). Effect of encouragement on walking test performance. Thorax, 39(11), 818–822. https://doi.org/10.1136/thx.39.11.818

15- Gadesmann, M., & Miller, N. (2008). Reliability of speech diadochokinetic test measurement. *International journal of language & communication disorders*, *43*(1), 41–54. https://doi.org/10.1080/13682820701234444

16- Martin, L., Hutchens, M., Hawkins, C., & Radnov, A. (2017). How much do clinical trials cost?. *Nature reviews. Drug discovery*, *16*(6), 381–382. https://doi.org/10.1038/nrd.2017.70

17- Abu-Baker, A., Kharma, N., Perreault, J., Grant, A., Shekarabi, M., Maios, C., Dona, M., Neri, C., Dion, P. A., Parker, A., Varin, L., & Rouleau, G. A. (2019). RNA-Based Therapy Utilizing Oculopharyngeal Muscular Dystrophy Transcript Knockdown and Replacement. *Molecular therapy. Nucleic acids*, *15*, 12–25. https://doi.org/10.1016/j.omtn.2019.02.003

18- Strings-Ufombah, V., Malerba, A., Kao, S. C., Harbaran, S., Roth, F., Cappellari, O., Lu-Nguyen, N., Takahashi, K., Mukadam, S., Kilfoil, G., Kloth, C., Roelvink, P., Dickson, G., Trollet, C., & Suhy, D. (2021). BB-301: a silence and replace AAV-based vector for the treatment of oculopharyngeal muscular dystrophy. *Molecular therapy. Nucleic acids*, *24*, 67–78. https://doi.org/10.1016/j.omtn.2021.02.017

19- Willcocks, R. J., Rooney, W. D., Triplett, W. T., Forbes, S. C., Lott, D. J., Senesac, C. R., Daniels, M. J., Wang, D. J., Harrington, A. T., Tennekoon, G. I., Russman, B. S., Finanger, E. L., Byrne, B. J., Finkel, R. S., Walter, G. A., Sweeney, H. L., & Vandenborne, K. (2016). Multicenter prospective longitudinal study of magnetic resonance biomarkers in a large duchenne muscular dystrophy cohort. *Annals of neurology*, *79*(4), 535–547. https://doi.org/10.1002/ana.24599

20- Ghasemi, M., Emerson, C. P., Jr, & Hayward, L. J. (2022). Outcome Measures in Facioscapulohumeral Muscular Dystrophy Clinical Trials. Cells, 11(4), 687. https://doi.org/10.3390/cells11040687

21- Willis, T. A., Hollingsworth, K. G., Coombs, A., Sveen, M. L., Andersen, S., Stojkovic, T., Eagle, M., Mayhew, A., de Sousa, P. L., Dewar, L., Morrow, J. M., Sinclair, C. D., Thornton, J. S., Bushby, K., Lochmüller, H., Hanna, M. G., Hogrel, J. Y., Carlier, P. G., Vissing, J., & Straub, V. (2013). Quantitative muscle MRI as an assessment tool for monitoring disease progression in LGMD2I: a multicentre longitudinal study. *PloS one*, *8*(8), e70993. https://doi.org/10.1371/journal.pone.0070993

22- Wokke, B. H., Bos, C., Reijnierse, M., van Rijswijk, C. S., Eggers, H., Webb, A., Verschuuren, J. J., & Kan, H. E. (2013). Comparison of dixon and T1-weighted MR methods to assess the degree of fat infiltration in duchenne muscular dystrophy patients. *Journal of magnetic resonance imaging : JMRI*, *38*(3), 619–624. https://doi.org/10.1002/jmri.23998

23-Andersen G, Dahlqvist JR, Vissing CR, Heje K, Thomsen C, Vissing J. MRI as outcome measure in facioscapulohumeral muscular dystrophy: 1-year follow-up of 45 patients. J Neurol. 2017;264(3):438-447. doi:10.1007/s00415-016-8361-3

24- Wang, L. H., Shaw, D. W. W., Faino, A., Budech, C. B., Lewis, L. M., Statland, J., Eichinger, K., Tapscott, S. J., Tawil, R. N., & Friedman, S. D. (2021). Longitudinal study of MRI and functional outcome measures in facioscapulohumeral muscular dystrophy. *BMC musculoskeletal disorders*, *22*(1), 262. https://doi.org/10.1186/s12891-021-04134-7

25- Vandenborne, K., Walter, G. A., Straub, V., Willcocks, R. J., Forbes, S. C., Mercuri, E. M., Muntoni, F., Ding, K., Ennamuri, S., Reid, C., Murphy, A. P., Manfrini, M., Mendell, J. R., Elkins, J. S., & Rodino-Klapac, L. R. (2025). Quantitative Muscle Magnetic Resonance Outcomes in Patients With Duchenne Muscular Dystrophy: An Exploratory Analysis From the EMBARK Randomized Clinical Trial. *JAMA neurology*, *82*(7), 734–744. https://doi.org/10.1001/jamaneurol.2025.0992

26- Burakiewicz, J., Sinclair, C. D. J., Fischer, D., Walter, G. A., Kan, H. E., & Hollingsworth, K. G. (2017). Quantifying fat replacement of muscle by quantitative MRI in muscular dystrophy. *Journal of neurology*, *264*(10), 2053–2067. https://doi.org/10.1007/s00415-017-8547-3

27- Mul, K., Horlings, C. G. C., Vincenten, S. C. C., Voermans, N. C., van Engelen, B. G. M., & van Alfen, N. (2018). Quantitative muscle MRI and ultrasound for facioscapulohumeral muscular dystrophy: complementary imaging biomarkers. *Journal of neurology*, *265*(11), 2646–2655. https://doi.org/10.1007/s00415-018-9037-y

28- Poliachik, S. L., Friedman, S. D., Carter, G. T., Parnell, S. E., & Shaw, D. W. (2012). Skeletal muscle edema in muscular dystrophy: clinical and diagnostic implications. *Physical medicine and rehabilitation clinics of North America*, *23*(1), 107–xi. https://doi.org/10.1016/j.pmr.2011.11.016

29- Nuñez-Peralta, C., Alonso-Pérez, J., Llauger, J., Segovia, S., Montesinos, P., Belmonte, I., Pedrosa, I., Montiel, E., Alonso-Jiménez, A., Sánchez-González, J., Martínez-Noguera, A., Illa, I., & Díaz-Manera, J. (2020). Follow-up of late-onset Pompe disease patients with muscle magnetic resonance imaging reveals increase in fat replacement in skeletal muscles. *Journal of cachexia, sarcopenia and muscle*, *11*(4), 1032–1046. https://doi.org/10.1002/jcsm.12555

30- Schrama, E. J., Hooijmans, M. T., van de Velde, N. M., Niks, E. H., Kan, H. E., & Cameron, D. (2025). Skeletal Muscle Membrane Permeability Markers Derived From ^{31}P-MRS May Reflect Disease Activity in Becker Muscular Dystrophy. *NMR in biomedicine*, *38*(11), e70155. https://doi.org/10.1002/nbm.70155

31- Bray, T. J., Chouhan, M. D., Punwani, S., Bainbridge, A., & Hall-Craggs, M. A. (2018). Fat fraction mapping using magnetic resonance imaging: insight into pathophysiology. *The British journal of radiology*, *91*(1089), 20170344. https://doi.org/10.1259/bjr.20170344

32- Higashiyama, T., Iwasa, M., & Ohji, M. (2017). Quantitative Analysis of Inflammation in Orbital Fat of Thyroid-associated Ophthalmopathy Using MRI Signal Intensity. *Scientific reports*, *7*(1), 16874. https://doi.org/10.1038/s41598-017-17257-6

33- Theodorou, D. J., Theodorou, S. J., Saba, L., & Kakitsubata, Y. (2022). Skeletal Muscle Disease: Imaging Findings Simplified. *Cureus*, *14*(9), e29655. https://doi.org/10.7759/cureus.29655

34- Paoletti, M., Pichiecchio, A., Cotti Piccinelli, S., Tasca, G., Berardinelli, A. L., Padovani, A., & Filosto, M. (2019). Advances in Quantitative Imaging of Genetic and Acquired Myopathies: Clinical Applications and Perspectives. *Frontiers in neurology*, *10*, 78. https://doi.org/10.3389/fneur.2019.00078

35- Dahlqvist, J. R., Salim, R., Thomsen, C., & Vissing, J. (2020). A quantitative method to assess muscle edema using short TI inversion recovery MRI. Scientific Reports, 10(1), Article 7246 . https://doi.org/10.1038/s41598-020-64287-8

36- Wang, F., Fang, S., Li, J., Yuan, L., Hou, B., Zhu, J., Jiao, Y., Liu, Z., Qian, M., Santini, F., Wang, Q., Chen, L., & Feng, F. (2023). Correlation analysis of quantitative MRI measurements of thigh muscles with histopathology in patients with idiopathic inflammatory myopathy. *European radiology experimental*, *7*(1), 51. https://doi.org/10.1186/s41747-023-00350-z

37- Englund, E. K., Reiter, D. A., Shahidi, B., & Sigmund, E. E. (2022). Intravoxel Incoherent Motion Magnetic Resonance Imaging in Skeletal Muscle: Review and Future Directions. Journal of magnetic resonance imaging : JMRI, 55(4), 988–1012. https://doi.org/10.1002/jmri.27875

38- Baliyan, V., Das, C. J., Sharma, R., & Gupta, A. K. (2016). Diffusion weighted imaging: Technique and applications. *World journal of radiology*, *8*(9), 785–798. https://doi.org/10.4329/wjr.v8.i9.785

39- Alonso-Jimenez, A., Kroon, R. H. M. J. M., Alejaldre-Monforte, A., Nuñez-Peralta, C., Horlings, C. G. C., van Engelen, B. G. M., Olivé, M., González, L., Verges-Gil, E., Paradas, C., Márquez, C., Garibaldi, M., Gallano, P., Rodriguez, M. J., Gonzalez-Quereda, L., Dominguez Gonzalez, C., Vissing, J., Fornander, F., Eisum, A. V., García-Sobrino, T., … Diaz-Manera, J. (2019). Muscle MRI in a large cohort of patients with oculopharyngeal muscular dystrophy. *Journal of neurology, neurosurgery, and psychiatry*, *90*(5), 576–585. https://doi.org/10.1136/jnnp-2018-319578

40- Kroon, R. H. M. J. M., Kalf, J. G., de Swart, B. J. M., Heskamp, L., de Rooy, J. W. J., van Engelen, B. G. M., & Horlings, C. G. C. (2024). Muscle MRI in Patients With Oculopharyngeal Muscular Dystrophy: A Longitudinal Study. *Neurology*, *102*(1), e207833. https://doi.org/10.1212/WNL.0000000000207833

41- Fischmann, A., Hafner, P., Fasler, S., Gloor, M., Bieri, O., Studler, U., & Fischer, D. (2012). Quantitative MRI can detect subclinical disease progression in muscular dystrophy. *Journal of neurology*, *259*(8), 1648–1654. https://doi.org/10.1007/s00415-011-6393-2

42- van der Sluijs, B. M., Lassche, S., Knuiman, G. J., Kusters, B., Heerschap, A., Hopman, M., Schreuder, T. H., van Engelen, B. G. M., & Voermans, N. C. (2017). Involvement of pelvic girdle and proximal leg muscles in early oculopharyngeal muscular dystrophy. *Neuromuscular disorders : NMD*, *27*(12), 1099–1105. https://doi.org/10.1016/j.nmd.2017.09.010

43- Melkus, G., Sampaio, M. L., Smith, I. C., Rakhra, K. S., Bourque, P. R., Breiner, A., Zwicker, J., Lochmüller, H., Brais, B., & Warman-Chardon, J. (2023). Quantitative vs qualitative muscle MRI: Imaging biomarker in patients with Oculopharyngeal Muscular Dystrophy (OPMD). *Neuromuscular disorders : NMD*, *33*(1), 24–31. https://doi.org/10.1016/j.nmd.2022.09.010

44- Warman Chardon, J., Díaz-Manera, J., Tasca, G., Bönnemann, C. G., Gómez-Andrés, D., Heerschap, A., Mercuri, E., Muntoni, F., Pichiecchio, A., Ricci, E., Walter, M. C., Hanna, M., Jungbluth, H., Morrow, J. M., Fernández-Torrón, R., Udd, B., Vissing, J., Yousry, T., Quijano-Roy, S., Straub, V., … MYO-MRI Working Group (2019). MYO-MRI diagnostic protocols in genetic myopathies. *Neuromuscular disorders : NMD*, *29*(11), 827–841. https://doi.org/10.1016/j.nmd.2019.08.011

45- Warman-Chardon, J., Diaz-Manera, J., Tasca, G., Straub, V., & MRI workshop study group (2020). 247th ENMC International Workshop: Muscle magnetic resonance imaging - Implementing muscle MRI as a diagnostic tool for rare genetic myopathy cohorts. Hoofddorp, The Netherlands, September 2019. *Neuromuscular disorders : NMD*, *30*(11), 938–947. https://doi.org/10.1016/j.nmd.2020.08.360

46- Venturelli, N., Tordjman, M., Ammar, A., Chetrit, A., Renault, V., & Carlier, R. Y. (2023). Contribution of muscle MRI for diagnosis of myopathy. *Revue neurologique*, *179*(1-2), 61–80. https://doi.org/10.1016/j.neurol.2022.12.002

47- Schober, P., Boer, C., & Schwarte, L. A. (2018). Correlation Coefficients: Appropriate Use and Interpretation. Anesthesia and analgesia, 126(5), 1763–1768. https://doi.org/10.1213/ANE.0000000000002864

48- Iima, M., & Le Bihan, D. (2016). Clinical Intravoxel Incoherent Motion and Diffusion MR Imaging: Past, Present, and Future. *Radiology*, *278*(1), 13–32. https://doi.org/10.1148/radiol.2015150244

49- Ran, J., Liu, Y., Sun, D., Morelli, J., Zhang, P., Wu, G., Sheng, Y., Xie, R., Zhang, X., & Li, X. (2016). The diagnostic value of biexponential apparent diffusion coefficients in myopathy. *Journal of neurology*, *263*(7), 1296–1302. https://doi.org/10.1007/s00415-016-8139-7

50- Ran, J., Dai, B., Liu, C., Zhang, H., Li, Y., Hou, B., & Li, X. (2022). The diagnostic value of T2 map, diffusion tensor imaging, and diffusion kurtosis imaging in differentiating dermatomyositis from muscular dystrophy. *Acta radiologica (Stockholm, Sweden : 1987)*, *63*(4), 467–473. https://doi.org/10.1177/0284185121999006

51- Forsting, J., Rohm, M., Froeling, M., Güttsches, A. K., Südkamp, N., Roos, A., Vorgerd, M., Schlaffke, L., & Rehmann, R. (2022). Quantitative muscle MRI captures early muscle degeneration in calpainopathy. *Scientific reports*, *12*(1), 19676. https://doi.org/10.1038/s41598-022-23972-6

52- Barzaghi, L., Paoletti, M., Monforte, M., Bortolani, S., Bonizzoni, C., Thorsten, F., Bergsland, N., Santini, F., Deligianni, X., Tasca, G., Ballante, E., Figini, S., Ricci, E., & Pichiecchio, A. (2024). Muscle diffusion tensor imaging in facioscapulohumeral muscular dystrophy. *Muscle & nerve*, *70*(2), 248–256. https://doi.org/10.1002/mus.28179

53- Liu, Y. J., Tsai, T. S., Li, Y. H., Peng, J. H., Chang, H. C., Peng, H. H., Lee, Y. C., Lee, T. Y., Liou, C. H., Lin, T. F., Chew, F. Y., Chou, R. H., & Juan, C. J. (2024). Understanding ADC variation by fat content effect using a dual-function MRI phantom. *European radiology experimental*, *8*(1), 19. https://doi.org/10.1186/s41747-023-00414-0

54- Wang, J., Yang, Z., Luo, M., Xu, C., Du, M., & Liu, Y. (2022). Value of Intravoxel Incoherent Motion (IVIM) Imaging for Differentiation between Intrahepatic Cholangiocarcinoma and Hepatocellular Carcinoma. *Contrast media & molecular imaging*, *2022*, 1504463. https://doi.org/10.1155/2022/1504463

55- Shen, M., Lin, X., Yang, C., Zhou, Z., Chen, S., Yin, Y., Long, L., Huang, L., Yang, Z., Wang, R., & Kang, M. (2024). Potential predictive value of IVIM MR for xerostomia in nasopharyngeal carcinoma. *Radiotherapy and oncology : journal of the European Society for Therapeutic Radiology and Oncology*, *197*, 110323. https://doi.org/10.1016/j.radonc.2024.110323

56- Ran, J., Yin, C., Liu, C., Li, Y., Hou, B., Morelli, J. N., Dai, B., & Li, X. (2021). The Diagnostic Value of MR IVIM and T2 Mapping in Differentiating Autoimmune Myositis From Muscular Dystrophy. *Academic radiology*, *28*(6), e182–e188. https://doi.org/10.1016/j.acra.2020.04.022

57- Yamashita S. (2021). Recent Progress in Oculopharyngeal Muscular Dystrophy. *Journal of clinical medicine*, *10*(7), 1375. https://doi.org/10.3390/jcm10071375

58- Subhawong, T. K., Jacobs, M. A., & Fayad, L. M. (2014). Diffusion-weighted MR imaging for characterizing musculoskeletal lesions. *Radiographics : a review publication of the Radiological Society of North America, Inc*, *34*(5), 1163–1177. https://doi.org/10.1148/rg.345140190

59- Kroon, R. H. M. J. M., Kalf, J. G., Meijers, R. L., de Swart, B. J. M., Cameron, I. G. M., Doorduin, J., van Alfen, N., van Engelen, B. G. M., & Horlings, C. G. C. (2022). Muscle ultrasound is a sensitive biomarker in oculopharyngeal muscular dystrophy. *Muscle & nerve*, *66*(4), 453–461. https://doi.org/10.1002/mus.27679

60- Meyer, H. J., Ziemann, O., Kornhuber, M., Emmer, A., Quäschling, U., Schob, S., & Surov, A. (2018). Apparent diffusion coefficient (ADC) does not correlate with different serological parameters in myositis and myopathy. Actaradiologica(Stockholm,Sweden:1987), 59(6),694–699. https://doi.org/10.1177/0284185117731448

61- Malartre, S., Bachasson, D., Mercy, G., Sarkis, E., Anquetil, C., Benveniste, O., & Allenbach, Y. (2021). MRI and muscle imaging for idiopathic inflammatory myopathies. *Brain pathology (Zurich, Switzerland)*, *31*(3), e12954. https://doi.org/10.1111/bpa.12954

62- Mann, C. J., Perdiguero, E., Kharraz, Y., Aguilar, S., Pessina, P., Serrano, A. L., & Muñoz-Cánoves, P. (2011). Aberrant repair and fibrosis development in skeletal muscle. *Skeletal muscle*, *1*(1), 21. https://doi.org/10.1186/2044-5040-1-21

63- Rauh, S. S., Baudin, P. Y., Stojkovic, T., Birnbaum, S., Decostre, V., Zanfongnon, R. L., Fromes, Y., Hooijmans, M. T., Strijkers, G. J., Hogrel, J. Y., Olivier, S., Marty, B., & Reyngoudt, H. (2025). Multi-parametric

quantitative MRI of the lower limb muscles in a longitudinal study of limb-girdle muscular dystrophy R9. *PloS one*, *20*(4), e0321463. https://doi.org/10.1371/journal.pone.0321463

64- Paoletti, M., Monforte, M., Barzaghi, L., Tasca, G., Bergsland, N., Faggioli, A., Solazzo, F., Manco, G., Bortolani, S., Torchia, E., Ravera, B., Deligianni, X., Santini, F., Ballante, E., Figini, S., Tartaglione, T., Ricci, E., & Pichiecchio, A. (2025). Natural history of facioscapulohumeral muscular dystrophy evaluated by multiparametric quantitative MRI: a prospective cohort study. *Journal of neurology*, *272*(4), 306. https://doi.org/10.1007/s00415-025-13062-8

65- Kekou, K., Papadopoulos, C., Svingou, M., Chrysanthou-Piterou, M., Nitsa, E., Veltra, D., Marinakis, N., Tilemis, F. N., Dimitrios, P., Arnaoutoglou, M., Moschou, M., Xirou, S., Bakirtzis, C., Tsivgoulis, G., Papadimas, G. K., & Sofocleous, C. (2025). Insights into the heterogeneity of oculopharyngeal muscular dystrophy. *Neurogenetics*, *26*(1), 68. https://doi.org/10.1007/s10048-025-00849-0

66- Yanagisawa, O., Shimao, D., Maruyama, K., Nielsen, M., Irie, T., & Niitsu, M. (2009). Diffusion-weighted magnetic resonance imaging of human skeletal muscles: gender-, age- and muscle-related differences in apparent diffusion coefficient. Magnetic resonance imaging, 27(1), 69–78. https://doi.org/10.1016/j.mri.2008.05.011

67- Heskamp, L., Ogier, A., Bendahan, D., & Heerschap, A. (2022). Whole-muscle fat analysis identifies distal muscle end as disease initiation site in facioscapulohumeral muscular dystrophy. *Communications medicine*, *2*(1), 155. https://doi.org/10.1038/s43856-022-00217-1

68- Riem, L., DuCharme, O., Cousins, M., Feng, X., Kenney, A., Morris, J., Tapscott, S. J., Tawil, R., Statland, J., Shaw, D., Wang, L., Walker, M., Lewis, L., Jacobs, M. A., Leung, D. G., Friedman, S. D., & Blemker, S. S. (2024). AI driven analysis of MRI to measure health and disease progression in FSHD. *Scientific reports*, *14*(1), 15462. https://doi.org/10.1038/s41598-024-65802-x

69- Carlier, P. G., Marty, B., Scheidegger, O., Loureiro de Sousa, P., Baudin, P. Y., Snezhko, E., & Vlodavets, D. (2016). Skeletal Muscle Quantitative Nuclear Magnetic Resonance Imaging and Spectroscopy as an Outcome Measure for Clinical Trials. *Journal of neuromuscular diseases*, *3*(1), 1–28. https://doi.org/10.3233/JND-160145

70- Kim, H., Yong, S. Y., Otgonbaatar, C., & Nam, S. W. (2024). Intravoxel Incoherent Motion Diffusion-Weighted MRI, Fat Quantification, and Electromyography: Correlation in Polymyositis and Dermatomyositis. *Tomography (Ann Arbor, Mich.)*, *10*(3), 368–377. https://doi.org/10.3390/tomography10030029

71- Janssen, B. H., Voet, N. B., Nabuurs, C. I., Kan, H. E., de Rooy, J. W., Geurts, A. C., Padberg, G. W., van Engelen, B. G., & Heerschap, A. (2014). Distinct disease phases in muscles of facioscapulohumeral dystrophy patients identified by MR detected fat infiltration. *PloS one*, *9*(1), e85416. https://doi.org/10.1371/journal.pone.0085416

72- Compston A. (2010). Aids to the investigation of peripheral nerve injuries. Medical Research Council: Nerve Injuries Research Committee. His Majesty's Stationery Office: 1942; pp. 48 (iii) and 74 figures and 7 diagrams; with aids to the examination of the peripheral nervous system. By Michael O'Brien for the Guarantors of Brain. Saunders Elsevier: 2010; pp. [8] 64 and 94 Figures. Brain : a journal of neurology, 133(10), 2838–2844. https://doi.org/10.1093/brain/awq270

73- Cleveland, W. S., & Devlin, S. J. (1988). Locally Weighted Regression: An Approach to Regression Analysis by Local Fitting. Journal of the American Statistical Association, 83(403), 596–610. https://doi.org/10.1080/01621459.1988.10478639

74- Lin, L., & Aloe, A. M. (2021). Evaluation of various estimators for standardized mean difference in meta-analysis. *Statistics in medicine*, *40*(2), 403–426. https://doi.org/10.1002/sim.8781

75- Solbakken, G., Bjørnarå, B., Kirkhus, E., Nguyen, B., Hansen, G., Frich, J. C., & Ørstavik, K. (2019). MRI of trunk muscles and motor and respiratory function in patients with myotonic dystrophy type 1. *BMC neurology*, *19*(1), 135. https://doi.org/10.1186/s12883-019-1357-8

76- Brydges C. R. (2019). Effect Size Guidelines, Sample Size Calculations, and Statistical Power in Gerontology. *Innovation in aging*, *3*(4), igz036. https://doi.org/10.1093/geroni/igz036

77- Jalnefjord, O., & Björkman-Burtscher, I. M. (2024). Comparison of methods for intravoxel incoherent motion parameter estimation in the brain from flow-compensated and non-flow-compensated diffusion-encoded data. Magnetic resonance in medicine, 92(1), 303–318. https://doi.org/10.1002/mrm.30042

78- Wang, F., Zhang, H., Wu, C., Wang, Q., Hou, B., Sun, Y., Kober, T., Hilbert, T., Zhang, Y., Zeng, X., & Jin, Z. (2019). Quantitative T2 mapping accelerated by GRAPPATINI for evaluation of muscles in patients with myositis. The British journal of radiology, 92(1102), 20190109. https://doi.org/10.1259/bjr.20190109

79- Marty, B., Baudin, P. Y., Reyngoudt, H., Azzabou, N., Araujo, E. C., Carlier, P. G., & de Sousa, P. L. (2016). Simultaneous muscle water T2 and fat fraction mapping using transverse relaxometry with stimulated echo compensation. NMR in biomedicine, 29(4), 431–443. https://doi.org/10.1002/nbm.3459

80- Jungmann, P. M., Pfirrmann, C., & Federau, C. (2019). Characterization of lower limb muscle activation patterns during walking and running with Intravoxel Incoherent Motion (IVIM) MR perfusion imaging. *Magnetic resonance imaging*, *63*, 12–20. https://doi.org/10.1016/j.mri.2019.07.016

81-Faul, F., Erdfelder, E., Buchner, A., & Lang, A. G. (2009). Statistical power analyses using G*Power 3.1: tests for correlation and regression analyses. Behavior research methods, 41(4), 1149–1160. https://doi.org/10.3758/BRM.41.4.1149

Appendix

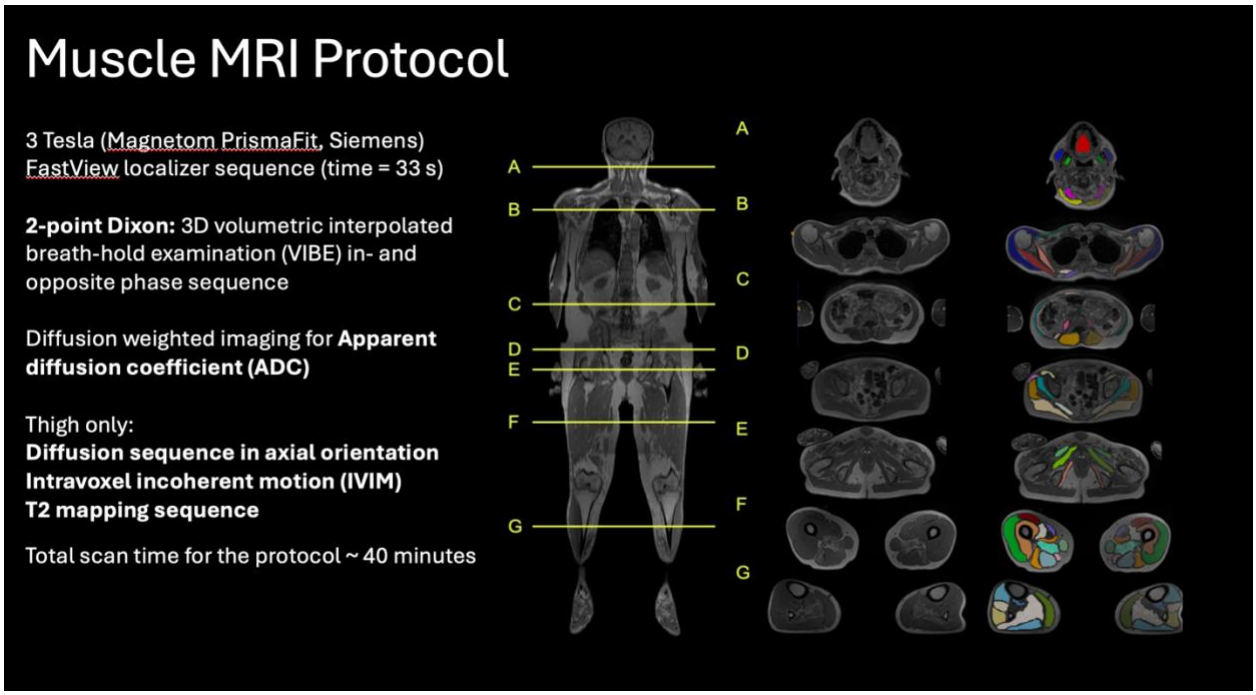

Supplementary Figure 1: Muscle MRI acquisition protocol and segmentation workflow.

Whole-body muscle MRI was performed at 3 Tesla using a FastView localizer, 2-point Dixon imaging, and diffusion-weighted imaging for ADC assessment. Additional IVIM and T2 mapping sequences were acquired in the thighs. The coronal image identifies the anatomical levels used for segmentation, and the axial images show representative unsegmented and segmented muscle slices. Manual segmentation was performed at predefined anatomical levels to extract quantitative MRI measures from individual muscles. This protocol allowed assessment of whole-body fat fraction and ADC, with additional thigh-level IVIM and T2 relaxation time analysis.

Supplementary Table 1. MRI parameters used for the different sequences in the study.

Sequence	STIR (TSE)	VIBE in- and opp phase	6-point PDFF	Whole Body Diffusion	IVIM (DWI)	T2 mapping
Orientation	Axial	Axial	Axial	Axial	Axial	Axial
Type	2D (multi-slice)	3D	3D	2D (multi-slice)	2D (multi-slice)	2D (multi-slice)
TR [ms]	3600	4	16	2900	2400	5000
TEs [ms]	30	1.29, 2.52	1.96, 3.80, 5.64, 7.48, 9.32, 11.16	39	37	8.5, 17.0, 25.5, 34.0, 42.5, 51.0
TI [ms]	220	-	-	SPAIR fat supression	SPAIR fat supression	SPAIR fat supression
Flip angle [degree]	120	8	3	90/180	90/180	90/180
FOV [mm x mm]	500 x 300	500 x 390	500 x 375	500 x 330	460 x 276	460 x 276
Matrix	256 x 155	416 x 325	224 x 168	200 x 132	180 x 108	208 x 125
Resolution [mm x mm]	1.95 x 1.95	1.2 x 1.2	2.2 x 2.2	2.5 x 2.5	2.6 x 2.6	2.2 x 2.2
Slice thickness [mm]	6	4	5	5	6	6
Number of slices	30	98	72	50	32	32
Parallel imaging factor	3	3	4	2	2	-
Simultaneous multi-slice factor	-	-	-	2	2	-
Bandwidth/pixel [Hz/pixel]	399	1000	1860	2500	1984	801
b-values [s/mm2] (averages)	-	-	-	50 (6); 800 (15)	0 (1), 20 (1), 30 (1), 80 (1), 100 (2), 200 (2), 400 (4), 600 (4), 800 (4), 1000 (4)	-
Time per bed position	55 s	55 s	48 s	1 min 34 s	3 min 56 s	4 min 52 s
Number of bed positions	5 (whole body)	5 (whole body)	5 (whole body)	5 (whole body)	1 (thigh)	1 (thigh)
Total time	4 min 35 s	4 min 35 s	4 min	7 min 50 s	3 min 56 s	4 min 52 s

Supplementary Table 2: Outline of muscles assessed by manual segmentation

OPMD — Mean muscle fat fraction (Upper body + trunk)	
Muscle	**Mean ± SD FF (%)**
Tongue	38.9 ± 20.3
External oblique	24.6 ± 11.1
Internal oblique	23.6 ± 10.9
Paraspinals (iliocostalis + longissimus + multifidus)	22.1 ± 12.3
Semispinalis	21.1 ± 12.8
Serratus anterior	19.4 ± 17.7
Psoas	18.4 ± 11.1
Splenius + trapezius	15.7 ± 10.1
Rectus abdominis	14.7 ± 7.1
Subscapularis	14.5 ± 11.5
Pectoralis major	14.1 ± 6.8
Quadratus lumborum	12.8 ± 5.3
Masticator	12.4 ± 8.2
Coracobrachialis	10.9 ± 7.8
Deltoid	10.1 ± 4.8
Teres minor + infraspinatus	9.4 ± 5.9
Rhomboid	8.8 ± 7.0
Trapezius	8.1 ± 3.9
Sternocleidomastoid	8.1 ± 2.6
Lateral pterygoid	5.8 ± 1.5

OPMD — Mean muscle fat fraction (Lower body)	
Muscle	**Mean ± SD FF (%)**
Adductor magnus	41.2 ± 28.9
Soleus	39.2 ± 25.9
Gluteus maximus	37.9 ± 23.2
Biceps femoris (long head)	33.8 ± 25.2
Semimembranosus	32.5 ± 22.3
Gluteus medius	26.9 ± 20.8
Gastrocnemius (medial)	26.4 ± 23.3
Semitendinosus	25.4 ± 19.7
Tensor fasciae latae	22.9 ± 17.1
Gluteus minimus	22.8 ± 21.1
Sartorius	21.1 ± 15.4
Iliacus	20.8 ± 24.5
Peroneus longus/brevis	20.1 ± 14.9
Gastrocnemius (lateral)	19.6 ± 18.9
Extensor digitorum longus	19.4 ± 16.2
Pectineus	18.9 ± 16.4
Adductor longus	18.0 ± 18.7
Tibialis posterior	17.9 ± 17.6
Biceps femoris (short head)	16.4 ± 10.0
Flexor hallucis longus	13.6 ± 13.6
Gracilis	13.2 ± 9.2
Obturator externus	12.4 ± 12.7
Piriformis	11.6 ± 9.6
Vastus intermedius	11.5 ± 11.5
Obturator internus	10.9 ± 9.8
Vastus medialis	10.2 ± 8.7
Tibialis anterior	9.6 ± 9.0
Vastus lateralis	8.1 ± 5.9
Rectus femoris	5.8 ± 3.0

This table summarizes the mean FF values across upper body/trunk and lower-body muscles in participants with OPMD. In the upper body and trunk, the tongue showed the highest mean FF, followed by the external oblique, internal oblique, paraspinal muscles, semispinalis, and serratus anterior. In the lower body, the highest mean FF values were seen in the adductor magnus, soleus, gluteus maximus, biceps femoris long head, and

semimembranosus. The table demonstrates a selective pattern of muscle involvement in OPMD, with greater fat replacement in specific muscles rather than uniform involvement across all muscles. Lower FF values were seen in muscles such as the lateral pterygoid in the upper body/face region and rectus femoris, vastus lateralis, and tibialis anterior in the lower body, suggesting relative sparing of these muscles in this cohort.

Supplemental Table 3: Correlation between MRC and qMRI measures

	FF-MRC	ADC-MRC	IVIM D-MRC	IVIM D*-MRC	IVIM F-MRC	T2 relaxation time-MRC
Calf	-0.74*	0.51*	NA	NA	NA	
Pelvis	-0.67*	0.56*	NA	NA	NA	
Thigh	-0.65*	0.48*	0.46*	0.41*	-0.19	0.21
Upper body+Face	-0.54*	0.23	NA	NA	NA	
Table exhibits spearman rank correlation between MRC sum score and q MRI * denotes p value <0.05 after Bonferroni correction						

This table shows Spearman rank correlations between regional qMRI measures and the total MRC muscle strength score. FF showed significant negative correlations with MRC score across all regions, including the calf, pelvis, thigh, and upper body/face, indicating that higher fat replacement was associated with lower muscle strength. ADC showed significant positive correlations with MRC score in the calf, pelvis, and thigh, suggesting that higher diffusivity was associated with better strength in these regions. In the thigh, IVIM D and IVIM D* also showed significant positive correlations with MRC score, while IVIM f and T2 relaxation time showed weak, non-significant correlations. Asterisks indicate correlations with $p < 0.05$ after Bonferroni correction.

Supplemental Table 4: This table summarizes the number and percentage of participants without available ADC values for each upper-body muscle in the OPMD cohort

Per-muscle ADC missingness (upper body, OPMD)

Percent of patients missing each muscle's ADC (both sides missing for bilateral muscles).

Muscle	Missing (n)	Total (n)	Percent missing (%)
Sternocleidomastoid	31	40	77.5
Splenius + trapezius	28	40	70.0
Lateral pterygoid	24	40	60.0
Masticator	24	40	60.0
Semispinalis	23	40	57.5
Tongue	14	40	35.0
Deltoid	12	40	30.0
Pectoralis major	11	40	27.5
Coracobrachialis	10	40	25.0
Rhomboid	6	40	15.0
Subscapularis	6	40	15.0
Teres minor + infraspinatus	6	40	15.0
Trapezius	6	40	15.0
Serratus anterior	5	40	12.5

The proportion of unavailable ADC data was highest in the sternocleidomastoid, followed by the splenius/trapezius region, lateral pterygoid, masticator, and semispinalis. The table demonstrates that ADC data availability varied by muscle, with lower availability in several craniofacial and upper-neck muscles compared with shoulder and upper-trunk muscles. This suggests that ADC assessment in the upper body was more limited in muscles that are smaller, anatomically complex, or more difficult to segment reliably.

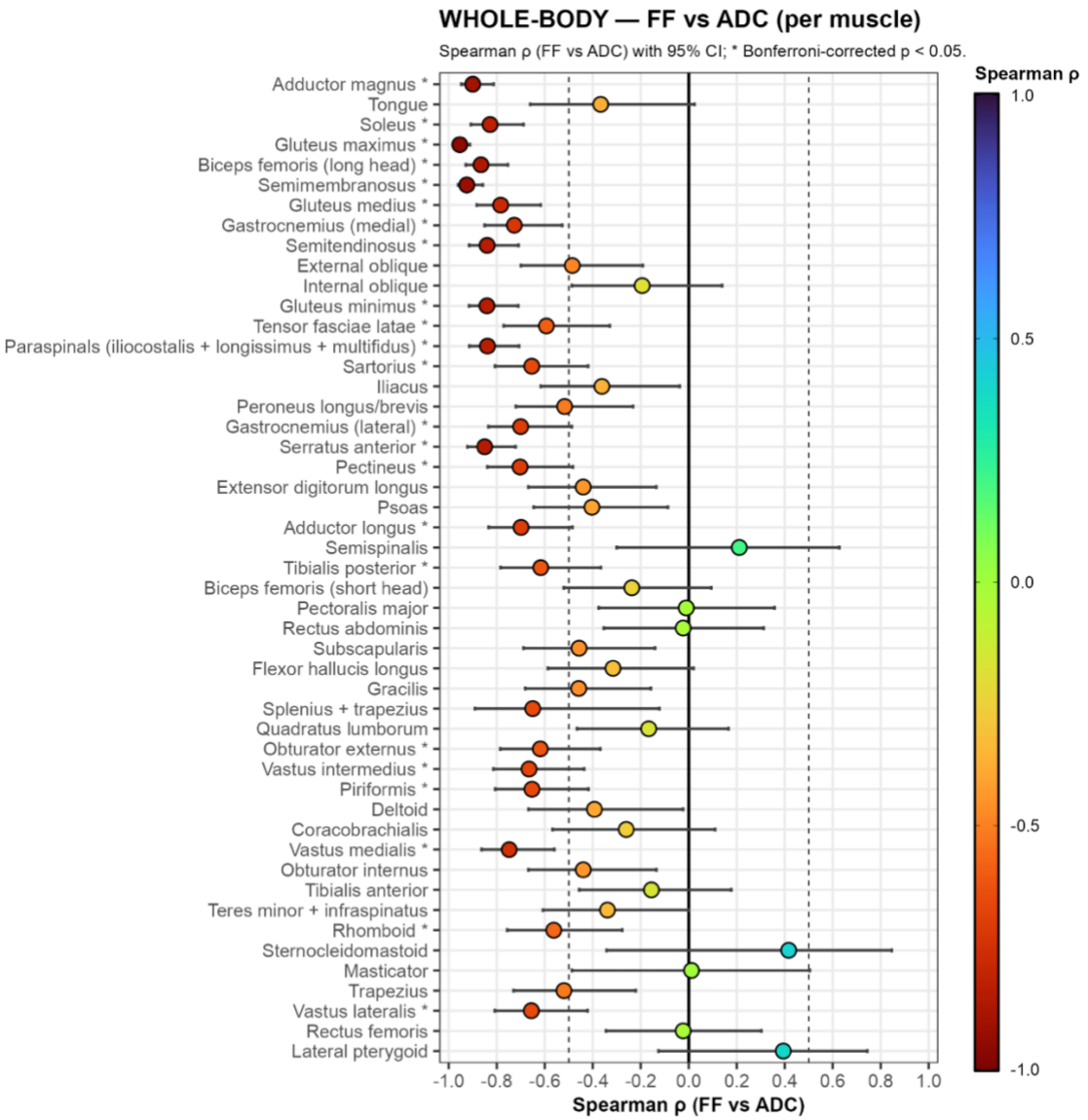

Supplemental Figure 2: High FF muscles in the thigh, pelvic and calf region have a stronger negative correlation with Apparent Diffusion Coefficient**.** High FF muscles in the thigh, pelvic and calf region have a stronger negative correlation with ADC: This forest plot shows the per-muscle Spearman correlation between fat fraction and ADC across whole-body muscles in participants with OPMD. Each point represents the correlation coefficient for an individual muscle, and the horizontal bars represent the 95% confidence intervals. Muscles are ordered by mean FF, with more fat-affected muscles shown toward the top of the figure. Asterisks indicate muscles with Bonferroni-corrected $p < 0.05$. Overall, the figure demonstrates that higher fat fraction is generally associated with lower

ADC values, with the strongest negative correlations seen in highly fat-replaced muscles such as the adductor magnus, soleus, gluteus maximus, biceps femoris long head, semimembranosus, gluteus medius, and gastrocnemius medialis. In contrast, several less fat-affected or technically more variable muscles showed weaker or non-significant associations. These findings support that the inverse relationship between FF and ADC is most evident in muscles with greater fat replacement.

Sentinel muscle selection and preliminary control sample size estimation

The five thigh muscles with the highest mean fat fraction in OPMD participants were identified as sentinel muscles: adductor magnus, biceps femoris (long head), semimembranosus, and semitendinosus. These muscles showed consistently higher FF values in OPMD than in controls. Using the participant-level mean fat fraction across these sentinel muscles, the observed between-group difference corresponded to a large, standardized effect size (Cohen's d = 1.111; Hedges' g = 1.094). Based on this effect size, a preliminary power analysis estimated that 14 participants per group would be required for 80% power, or 8 controls with the current OPMD participant sample size. Additional analysis would be required by widening the muscle pool and including more controls to assess the sample size of controls.

A

Sentinel high-FF thigh muscles in OPMD

Muscle	Mean FF in OPMD (%)	SD	Range
Adductor magnus	41.20	28.92	4.13–88.78
Biceps femoris (long head)	33.75	25.22	4.76–87.43
Semimembranosus	32.45	22.34	4.79–83.45
Semitendinosus	25.39	19.72	5.45–77.36
Sartorius	21.06	15.36	4.54–75.17

B

Sentinel high-FF thigh muscles in controls

Muscle	Mean FF in controls (%)	SD	Range
Adductor magnus	7.47	3.99	2.15–14.85
Biceps femoris (long head)	10.07	5.79	2.54–19.54
Semimembranosus	13.41	8.17	2.19–30.27
Semitendinosus	9.40	5.21	2.66–16.43
Sartorius	14.64	9.15	2.29–35.77

C

Sentinel-muscle control sample size summary

Item	Value
Sentinel muscles	AM; BL; SM; ST; SART
Observed OPMD n	40
Observed control n	12
Mean sentinel FF in OPMD (%)	30.77 ± 19.94 (5.96–78.76)
Mean sentinel FF in controls (%)	11.00 ± 5.62 (2.37–20.69)
Cohen d	1.111
Hedges g	1.094
Required n per group for 80% power	14
Required controls for 80% power with current OPMD n	8

Supplemental Figure 3: Sentinel muscle selection and preliminary control sample size estimation. (A) The five thigh muscles with the highest mean FF in OPMD were identified. For each muscle, the table shows the mean fat fraction, standard deviation, and range in OPMD. (B) The same sentinel muscles are shown in controls, with

corresponding mean fat fraction, standard deviation, and range. Across all five muscles, FF was lower in controls than in OPMD participants. (C) A participant-level sentinel muscle fat fraction was calculated as the mean across these five muscles. This summary table shows the observed OPMD and control sample sizes, the mean sentinel muscle FF in each group, and the standardized effect sizes (Cohen's d and Hedges' g) derived from the group difference.

Authorship for manuscript titled: The case report of Dual diagnosis of late onset facioscapulohumeral muscular dystrophy and myasthenia gravis

Tanay Satarkar, Ian C Smith, Ari Breiner, Gerd Melkus, Marcos L. Sampaio, Jodi Warman-Chardon

CRediT authorship contribution statement

Tanay Satarkar: Writing – original draft, chart review Ian Smith: Writing – original draft, review and editing. Ari Breiner: Patient investigation, review and editing. Gerd Melkus: Review and editing. Marcos Sampaio: review and editing. Jodi Warman-Chardon: Writing-original draft, patient investigation, review and editing.

Status: The case report of Dual diagnosis of late onset facioscapulohumeral muscular dystrophy and myasthenia gravis is accepted for publication and is in the production stage in the Annals of Indian academy of Neurology as of 21 June 2026.

Case report: Dual diagnosis of late onset facioscapulohumeral muscular dystrophy and myasthenia gravis

Dear Editor,

Facioscapulohumeral muscular dystrophy type-1 (FSHD) is the third most common inherited muscular dystrophy with an estimated prevalence of 1:8,000-1:22,000 [1]. FSHD is autosomal dominant and caused by a reduction in repeat units of D4Z4, a polymorphic repeat sequence located in the sub-telomeric region of chromosome 4 (4q35) [2]. FSHD presents with asymmetric facial, scapular, and humeral weakness; significant bulbar weakness (e.g., dysphagia, dysarthria, dysphonia) is considered atypical [1, 3].

Myasthenia gravis (MG) is an autoimmune, neuromuscular junction disorder with fluctuating and fatigable weakness involving ocular, bulbar, or proximal limb muscles. Impairment of neuromuscular transmission is typically caused by antibodies against the acetylcholine receptor (AChR), muscle specific tyrosine kinase, or low-density lipoprotein receptor–related protein [4]. though 8-15% of MG cases are seronegative MG responds to acetylcholinesterase inhibitors and immunosuppressants [1-10].

This letter describes a case of late-onset, genetically confirmed FSHD in an elderly male. He then developed mild chewing fatigability and dysphagia suggesting a coexisting neuromuscular junction disorder, and was diagnosed with AChR antibody positive MG. The emergence of fluctuating bulbar symptoms in a patient with FSHD should prompt reconsideration of the diagnosis or evaluation for a secondary condition [1-3, 5]. Attributing such features to FSHD disease progression alone may result in missing MG diagnosis and treatment, leading to poor clinical outcomes [1, 2]. We also review reports of coexisting FSHD and MG.

Case Presentation

A 78-year-old male presented with five-year history of slowly progressive facial and limb weakness, diffuse myalgias, elevated creatine kinase, and recurrent falls. His daughter had recently been diagnosed with FSHD at age 45. Family history was otherwise negative. He reported difficulty lifting objects, an inability to whistle, and sleeping with his eyes partially open. He described mild, intermittent dysphagia but denied aspiration, ptosis, and diplopia. Neurological examination showed no dysarthria or ptosis. He had significant bifacial weakness, particularly involving orbicularis oculi. There was no fatigable limb weakness or ptosis on initial exam. Medical Research Council strength scores for shoulder abduction were 4/5, bilaterally. He had asymmetric scapular winging and abdominal weakness. Hip flexion was 4-/5 on the left and 4/5 on the right. Genetic testing confirmed FSHD with 10 D4Z4 repeats on 4qA.

One month later, he presented with worsening dysphagia and fatigue with chewing. Examination showed known facial weakness and mild flaccid dysarthria. Nerve conduction studies were normal. Needle EMG revealed small, polyphasic motor units with early recruitment in proximal muscles, consistent with FSHD. However, 3 Hz

repetitive nerve stimulation showed a 24% decrement of the right ulnar motor response at abductor digit minimi and 49% decrement in the right facial motor response at nasalis. Anticipating MG, antibody testing was requested. A trial of pyridostigmine 30 mg three times daily resulted in clear symptomatic improvement., including reduced dysphagia, improved dysarthria, and less fatigue. After confirmation of seropositivity (AchR antibody titer 14.1 nmol/L, normal <0.4 nmol/L), intravenous immunoglobulin (IVIG) infusions (5 infusions, 60 g per dose) and prednisone (10 mg) were prescribed, with pyridostigmine continued at the same dose. All medications were well tolerated. During the following visits, prednisone and IVIG were discontinued as no further symptomatic improvement was seen but he continued to use pyridostigmine.

Discussion

Detecting coexistent genetic and acquired neuromuscular disorders remains challenging, especially with overlapping symptoms of facial and proximal weakness. Physicians often prematurely attribute new symptoms to the patient's existing disease, adhering to Occam's razor [2]. However, consideration of a secondary diagnosis is essential when atypical features are present. The timely identification of a treatable comorbidity—such as MG—can improve clinical outcomes and decrease the risk of rapid or severe deterioration. Some MG patients may present without significant ocular involvement [6].

We have summarized previously reported cases (n=22; Table 1) of concurrent FSHD and MG. In all cases, symptoms not typical of FSHD, such as ptosis, diplopia, or prominent bulbar weakness, provided important clinical clues towards the presence of a secondary disorder [1-10]. Diagnoses of MG were primarily supported by seropositivity (typically anti-AChR antibodies) [1-10] and by decrement of repetitive nerve stimulation [1, 5, 7, 8]. Although jitter on single fibre EMG can be present in muscular dystrophy, jitter [1, 6, 9] also may indicate a disorder of impaired neuromuscular transmission in patients with FSHD. The current case, and previous reports of coexistent late-onset FSHD and MG [1-10], highlight the importance of considering neuromuscular junction disorders in the differential when fatigable weakness is identified, even when a muscular dystrophy has been genetically confirmed. The late diagnosis of FSHD in our patient (in the 8th decade of life) was atypical, likely because of mild, slowly progressive symptoms, previously attributed to normal aging. This case also highlights a potential source of diagnostic bias: subtle manifestations of muscle weakness in older adults may be overlooked or attributed to nonspecific age-related changes, leading to delays in accurate diagnosis and timely management. Importantly, patients with coexistent MG and FSHD respond well to standard MG therapies including pyridostigmine, IVIG, corticosteroids, or other immunosuppressants, with no worsening of FSHD symptoms reported [1-10].

The pathophysiology of MG development in patients with FSHD remains unclear [1, 3, 5, 9]. Chronic myofiber degeneration in muscular dystrophies has been speculated to promote autoimmunity by exposing self-antigens and breaking immune tolerance [1, 2, 4, 6, 7, 9]. Additionally, reports of MG coincident with muscular

dystrophies feature a disproportionately large number of cases with FSHD [8], and 10 patients with MG and FSHD were recently identified at a single center [4]. However, overlap of these two conditions is still rare, and it remains to be seen if co-occurrence of FSHD and MG is incidental rather than causal [2, 7, 9].

Conclusion

This case underscores the need to reassess new or worsening symptoms in patients with established neuromuscular disease, particularly for patients with FSHD, who may be at greater risk of developing an autoinflammatory condition. Fluctuating and rapid changes in weakness and bulbar dysfunction in FSHD should prompt evaluation for coexisting, potentially treatable conditions with important implications for management and outcomes.

References

[1] E. Filippelli, S. Barone, A. Granata, R. Nistico, P. Valentino, A case of facioscapulohumeral muscular dystrophy and myasthenia gravis with positivity of anti-Ach receptor antibody: a fortuitous association?, Neurol Sci 40(1) (2019) 195-197.
[2] A. Ketabforoush, R. Castoro, W.D. Arnold, R.J. Barohn, When Facioscapulohumeral dystrophy Meets Myasthenia gravis: Case Report and Literature Review, RRNMF Neuromuscular Journal 6(1) (2025) 32-36.
[3] F. Nauman, M.F.A. Hussain, A.Z. Burakgazi, The development of myasthenia gravis in a patient with facioscapulohumeral muscular dystrophy: case report and literature review, Neurol Int 11(3) (2019) 8191.
[4] G. Tammam, L. Villa, R. Lemmers, J. Pini, A. Slioui, L. Bouchareychas, Y. David, M.B. Ioncea, L. Salviati, M. Cavalli, A. Ezaru, A. Puma, J.J. Verschuuren, S.M. van der Maarel, S. Sacconi, Co-Occurrence of Myasthenia Gravis and Facioscapulohumeral Muscular Dystrophy: A Case Series and Review of Literature, Eur J Neurol 33(1) (2026) e70477.
[5] M. Asadollahi, B. Rezaiyan, H. Amjadi, A rare case of facioscapulohumeral muscular dystrophy and myasthenia gravis, Iran J Neurol 11(1) (2012) 28-9.
[6] R.J. Lane, F. Roncaroli, P. Charles, D.G. McGonagle, R.W. Orrell, Acetylcholine receptor antibodies in patients with genetic myopathies: clinical and biological significance, Neuromuscul Disord 22(2) (2012) 122-8.
[7] V. Sansone, D.S. Saperstein, R.J. Barohn, G. Meola, Concurrence of facioscapulohumeral muscular dystrophy and myasthenia gravis, Muscle Nerve 30(5) (2004) 679-80.
[8] A.R. Avallone, V. Di Stefano, L. Bevilacqua, P. Alonge, A. Lupica, S. Maccora, R. Monastero, S. Amabile, P. Barone, F. Brighina, C. Vinciguerra, AChR-seropositive myasthenia gravis in muscular dystrophy: diagnostic pitfalls and clinical management challenges, Neurol Sci 46(1) (2025) 125-132.
[9] A. McGonigal, A.M. Thomas, R.K. Petty, Facioscapulohumeral muscular dystrophy and myasthenia gravis co-existing in the same patient: a case report, J Neurol 249(2) (2002) 219-20.
[10] M. Guger, G. Caravias, W. Struhal, G. Ransmayr, Myasthenia gravis and facioscapulohumeral muscular dystrophy (FSHD) co-existing in one patient — A case report, Journal of the Neurological Sciences 333 (2013) E469-E470.